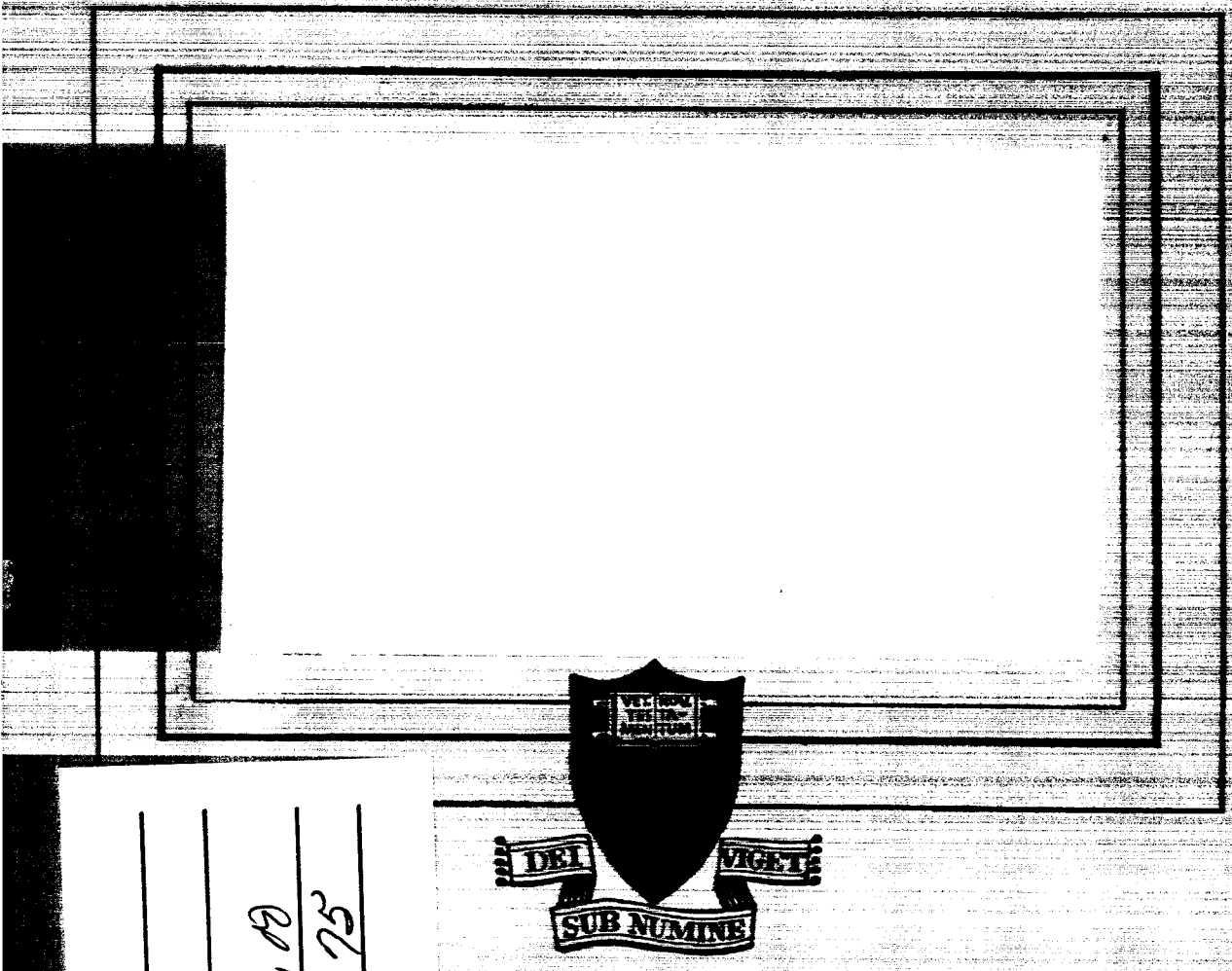

PRINCETON UNIVERSITY

DEPARTMENT OF AEROSPACE AND MECHANICAL SCIENCES

NATIONAL AERONAUTICS
AND SPACE ADMINISTRATION

Research Grant NsG-306-63

PULSED ELECTROMAGNETIC GAS ACCELERATION

Fifth Semi-Annual Progress Report

1 July 1964 to 31 December 1964

Report No. 634d

Prepared by: Robert G. Jahn
Robert G. Jahn
Associate Professor
and Research Leader

and: Woldemar v. Jaskowsky
Woldemar F. von Jaskowsky
Research Engineer

with contributions from the staff:

N. Black (Graduate-Assistant)
R. Burton (Graduate-Fellow)
J. Corr (Graduate-Assistant)
W. Ellis (Graduate-Assistant)
W. Hermann (Visiting Scholar)
E. Holzhauer (Visiting Scholar)
G. Rowell (Graduate-Fellow)
P. Turchi (University Scholar)
E. Wright (Graduate-Fellow)

29 January 1965

Guggenheim Laboratories for the Aerospace Propulsion Sciences
Department of Aerospace and Mechanical Sciences
PRINCETON UNIVERSITY
Princeton, New Jersey

ABSTRACT

20652

The ejection of the plasma produced in a pinch chamber from an axial orifice in one electrode is studied photographically, and with magnetic probes. The development of the discharge within the chamber is found to be disturbed very little by the presence of the large aperture in one electrode. A luminous front and current sheet are observed to diffract radially and axially outward through the orifice, establishing an exhaust plume which embodies large current densities and magnetic fields. The intense plasma column created by the pinch within the chamber also expands axially out through the orifice, eventually overtaking and piercing through the previously ejected diffracted front. In some cases the velocity of this axial expansion exceeds that of the prior interior radial motion, indicating significant recovery of the thermal energy resident in the pinch column.

A pulse-line device permitting the application of current waveforms of many shapes to a pinch discharge has been constructed and operated. Rectangular current pulses driven through the discharge are found to produce striking improvement in its dynamical characteristics, compared with similar discharges driven by a free-ringing capacitor bank. Elimination of secondary discharges, the attainment of plasma velocities four or five times higher than with the lumped bank, and an order of magnitude intensification of the interior current sheets are the most obvious improvements from a propulsion viewpoint.

Results of recent microwave and spectroscopic studies of closed-chamber pinch discharges are found to correlate well with each other, and with previously obtained information on current density and magnetic field distributions. Of particular interest is the identification of a severe rarefaction phase following the first reflection of the primary pinch at the chamber center line which drastically reduces the previously high electron density in the pinch column.

A variety of other related experiments and theoretical efforts round out the program. further

TABLE OF CONTENTS

		Page
	TITLE PAGE	i
	ABSTRACT	ii
	TABLE OF CONTENTS	iii
	LIST OF ILLUSTRATIONS	iv
I.	INTRODUCTION	1
II.	EXHAUST OF THE PINCHED PLASMA FROM AN AXIAL ORIFICE	2
III.	PULSE-FORMING NETWORK DISCHARGE STUDIES	31
IV.	MICROWAVE STUDIES	43
V.	SPECTROSCOPY	59
VI.	OTHER STUDIES, SUMMARY, AND PLANS	63
	REFERENCES	64
	APPENDIX A: Semi-Annual Statement of Expenditures	66

LIST OF ILLUSTRATIONS

Figure		Page
1	5" Plasma Pinch Apparatus with Exhaust Orifice	3
2	View of Pinch Exhaust Apparatus	4
3	Streak Photograph of Exhaust from 5" Pinch Discharge in 120 μ Argon Through 3/4" Diameter Orifice	6
4	Velocity of Exhausted Gas from Orifices of Different Diameter, in 120 μ Argon	7
5	Discharge Chamber with Orifice and Exhaust Chamber (Schematic)	8
6	Pinch Discharge Apparatus with Exhaust Chamber	9
7	Kerr Cell Photographs of Exhaust from Pinch Discharge in 120 μ Argon	11
8	Diagonal View of Pinch Discharge: 120 μ Argon, 4" Orifice	12
9	View Magnetic Probe in Discharge Chamber	14
10	Current Profiles 120 μ Argon, 4" Orifice; t = 0.4 μsec	15
11	Current Profiles 120 μ Argon, 4" Orifice; t = 1.2 μsec	16
12	Current Profiles 120 μ Argon, 4" Orifice; t = 2.0 μsec	17
13	Current Profiles 120 μ Argon, 4" Orifice; t = 2.8 μsec	18
14	Current Profiles 120 μ Argon, 4" Orifice; t = 4.0 μsec	19
15	View of Pinch Exhaust Apparatus with Pulse Line	20
16	Current Waveforms of Pinch Discharge	21
17	Current Profiles 120 μ Argon, 4" Orifice; t = 1.0 μsec	23

LIST OF ILLUSTRATIONS-contd.

Figure		Page
18	Current Profiles 120 μ Argon, 4" Orifice; t = 2.0 μsec	24
19	Current Profiles 120 μ Argon, 4" Orifice; t = 3.0 μsec	25
20	Current Profiles 120 μ Argon, 4" Orifice; t = 4.0 μsec	26
21	Current Profiles 120 μ Argon, 4" Orifice; t = 5.0 μsec	27
22	Current Profiles 120 μ Argon, 4" Orifice; t = 6.0 μsec	28
23	Kerr Cell Photographs of Exhaust from Constant Current Pinch in 120 μ Argon	29
24	Luminous Front Trajectories	30
25	Top View of Pulse Forming Network (Schematic)	32
26	Pulse Forming Network Cross Section (Schematic)	33
27	View of Pulse Forming Network	34
28	Typical Pulse Network Program Output	39
29	8" Pinch Discharge in 120 μ Argon for Two Current Waveforms	40
30	Comparison of Magnetic Probe Responses for Two Current Waveforms	42
31	8" Plasma Pinch Chamber with Electrode for μ-Wave Probing	44
32	70 GC Reflection at R/R_o = 0.75 120 μ Discharge	46
33	70 GC Reflection at Center of Chamber 120 μ Discharge	47
34	8" Pinch Discharge in Argon: Elapsed Time to Initial Intercept vs. Radial Position, 70 GC	48

LIST OF ILLUSTRATIONS-contd.

Figure		Page
35	8" Pinch Discharge in Argon: Time to 1/2 Max. Reflection of 70 GC	49
36	8" Pinch Discharge in Argon: Time to 1/2 Max. Reflection vs. Pressure, 70 GC	50
37	8" Pinch Discharge in Nitrogen: Δt_3, Time from Initial Intercept to 1/2 Max. Reflection vs. Pressure, 70 GC	52
38	Reflection Coefficient and Streak Picture in 8" Argon Discharge at 120 μ	54
39	Reflection Coefficient and Streak Picture in 8" Helium Discharge at 300 μ	55
40	Reflection Coefficient and Streak Picture in 8" Nitrogen Discharge at 100 μ	56
41	8" Pinch Discharge in Argon: Δt_7, Ionization Time vs. Radial Position, 70 GC	57
42	8" Pinch Discharge, "Typical" Ionization Time vs. Pressure, 70 GC	58
43	Maximum Continuum Intensity in Luminous Front at 4750 Å	61
44	Maximum Continuum Intensity in Center of Pinch at 4750 Å	62

I. INTRODUCTION

This program is devoted to a systematic study of the basic physical interactions which arise in pulsed plasma accelerators. Its past accomplishments and its status at the start of the present reporting period are discussed in the earlier semi-annual reports, and in several journal publications and technical society preprints, copies of all of which have previously been submitted to the project file (1-18). This report will confine itself entirely to the achievements of the past six months. For this purpose it is divided into the following sections:

Part II describes the study of the exhaust of a pinched plasma from an axial orifice. This is believed to be the first systematic examination of a plasma ejection process of this type, and brings the program one step closer to eventual implementation of a thrust-producing device. Part of this material was presented to the annual AIAA Aerospace Sciences Meeting on January 25, 1965, and is also available as preprint number 65-92 from that meeting. Additional results, obtained after submission of that paper, are included here.

Part III describes the analysis, design, construction, and first results of a pulse-forming network discharge apparatus. This device has permitted the application of a variety of current waveforms to the pinch discharge, rather than confining it to the typical ringing pulse. Early studies with a rectangular current waveform have shown increases in the discharge current sheet velocities by factors of 4 and 5 over the comparable ringing pulse cases. A computer program has been developed which aids in selecting the arrangements of network elements to produce the most interesting current waveforms.

Part IV summarizes the results of the microwave probing of the precursor and after-flow regions of closed-chamber discharges. These results have proven helpful in establishing the initial conditions for our three-fluid theoretical model of the current sheet, and are found to correlate well with previously obtained optical data.

Part V outlines the progress of the spectroscopic program during the reporting period. Although this work has not been a major emphasis, the measurements of continuum intensity throughout the chamber again have provided a valuable index of free electron density for purposes of other diagnostic experiments.

Part VI briefly summarizes other aspects of the program, including certain theoretical computations, and forecasts the activity for the next reporting period.

II. EXHAUST OF THE PINCHED PLASMA FROM AN AXIAL ORIFICE
(Jahn, vonJaskowsky, Burton)

Any pulsed plasma accelerator must accomplish a sequence of three physical operations: first, a sufficiently impermeable current sheet must be established in a proper geometric location; then, this current sheet must be accelerated stably by its own field into an ambient body of gas; and finally, the accelerated and heated body of gas must be ejected from the acceleration chamber. The first two processes have been studied in considerable detail for various accelerator geometries (1-16). The ejection process seems to have received comparatively little systematic study, although a variety of curious phenomenological observations have been reported in connection with the detachment of the plasma from the muzzle of coaxial guns and pinch engines.

The importance of the ejection process to the overall efficiency of the accelerator is evident enough, but reduction of the problem to its essential mechanisms is not entirely straightforward. At least three general questions can be defined: 1) to what extent does the existence of the exhaust orifice influence the development of the discharge within the acceleration chamber? 2) to what extent may random thermal energy resident in the plasma be recovered in directed motion upon expansion through the orifice? and 3) to what extent are current densities and magnetic fields present in and around the exhaust plume, thereby extending the acceleration process, or perhaps impeding the detachment of the plasma from the orifice? This subdivision of the problem becomes less clear-cut, however, when these questions are cast against the myriad of possible orifice sizes and shapes, and interior discharge characteristics.

In an effort to acquire some information on these questions, the 5" linear pinch discharge device, shown in Figs. 1, 2 and described in detail in an earlier report (13), is equipped with an assortment of interchangeable outer electrodes each containing a centered orifice of a particular diameter and profile. The discharge is driven by a bank of 15 - 1 μfd capacitors charged to 10 KV which ring down at about 400 KC, delivering about 300,000 amps peak current. The plasma generated by the radial implosion of the discharge current sheet is allowed to exhaust axially through the orifice into a large, cylindrical pyrex vessel, coaxial with the pinch chamber and orifice, and maintained at the same ambient pressure as the interior of the pinch chamber. The development of the exhaust plume, and the preceding development of the discharge within the chamber near the orifice, are then studied by Kerr-cell and streak photographs and by a series of magnetic probe traverses of the same regions, for ambient pressures of 30 μ, 120 μ, 480 μ, and 1920 μ of argon.

IPPS-JPR 4000-64

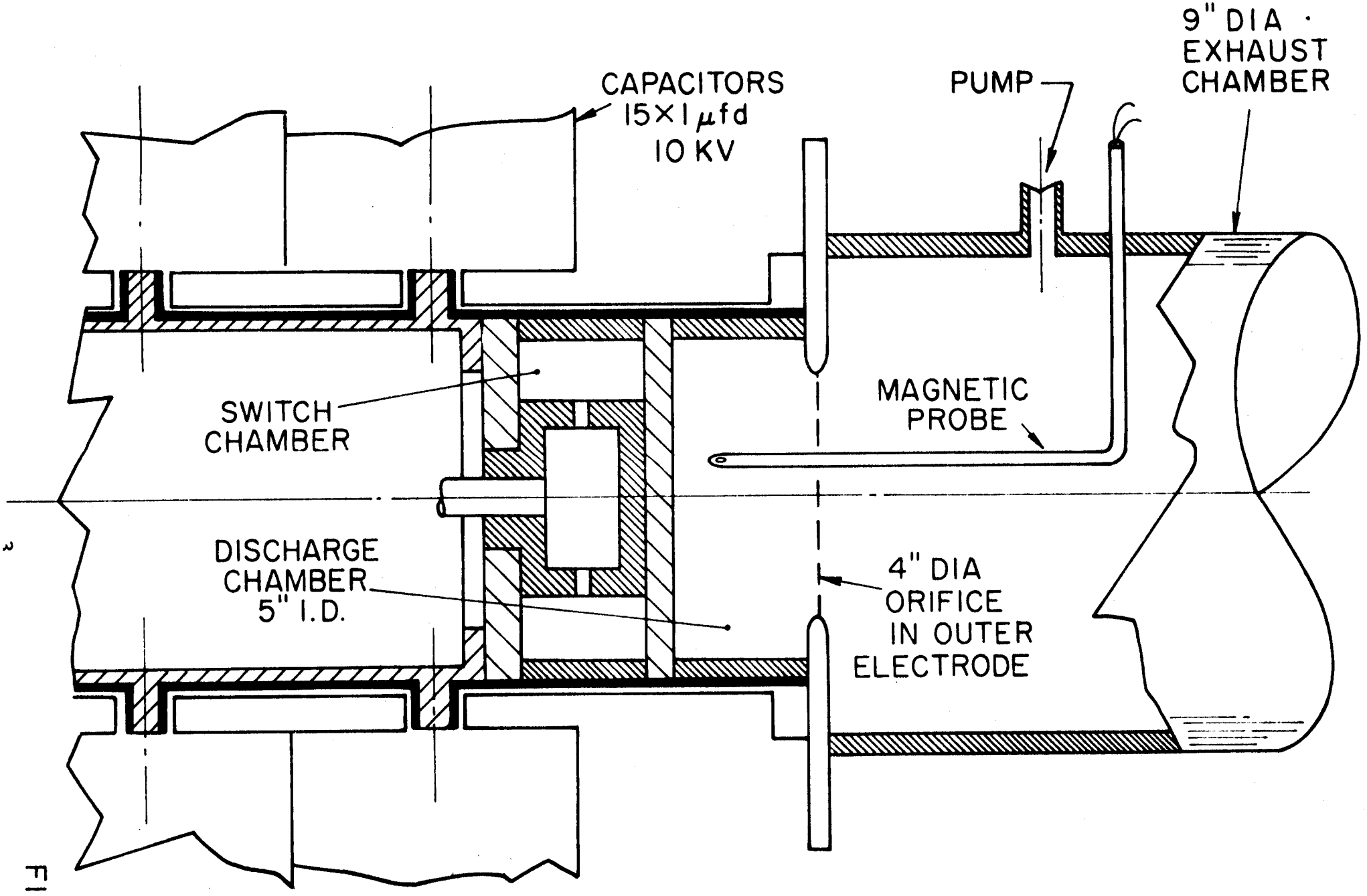

FIGURE 1

5" PLASMA PINCH APPARATUS WITH EXHAUST ORIFICE

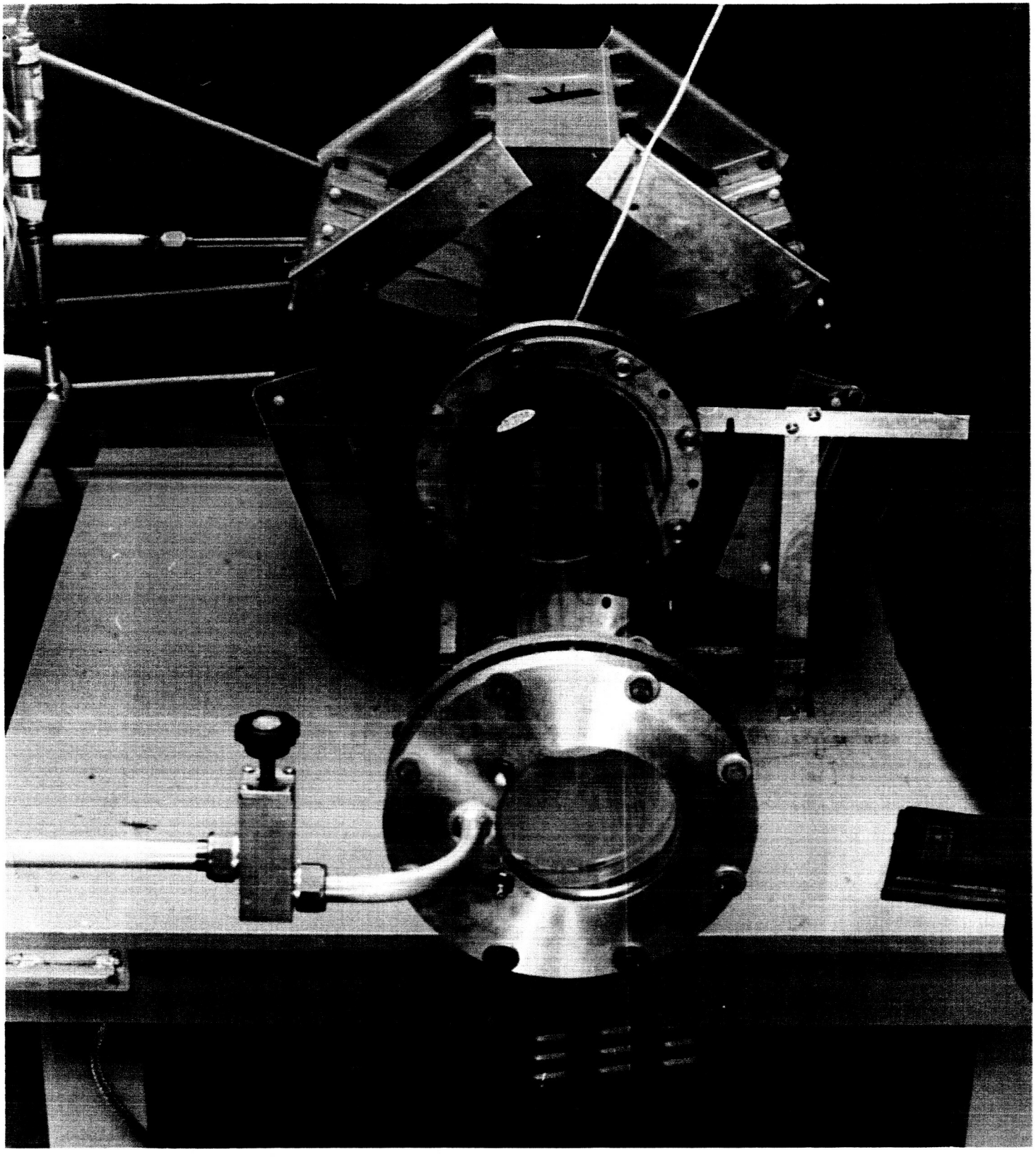

VIEW OF PINCH EXHAUST APPARATUS

FIGURE 2

To determine the optimum orifice configuration on which to conduct the detailed experiments, the exhaust plumes emerging from various diameter apertures were first surveyed photographically. Orifices of 3/8", 3/4", 1-1/2", 2", 3", and 4" were allowed to discharge into a 6" diameter x 24" long pyrex exhaust tank, through which streak photographs mapping the axial progression of the exhaust luminosity along the centerline, and radial view Kerr cell photographs displaying the entire plume geometry at selected times, were obtained. A typical streak photograph is shown in Fig. 3. In each case, the main luminous leading edge of the exhaust is observed to emerge with a particular initial speed, and then to decelerate at a rate characteristic of the hole size, and of the ambient pressure. Figure 4 summarizes the observed behavior of these trajectories for discharges in 120 μ argon. For the smaller size holes, the initial exhaust speeds are nearly the same, but the persistence of the leading edge speed downstream of the orifice clearly improves with increasing hole diameter. To check whether this effect could be ascribed to the lack of an expansion profile within these orifices, simple conical nozzles with throat to exit diameters of 3/8":1½"; and 3/4":1½" were tried, and found to yield trajectories indistinguishable from those of the straight orifices of the same diameter as their throats. The tentative conclusion was that the exhaust process was primarily limited by the minimum diameter of the orifice, rather than by the details of its contour. This conclusion was supported by full-field photographs obtained later of the large orifice exhaust patterns.

Returning to the straight orifices, the streak photographs for the larger diameter holes reveal substantially higher initial speeds, as shown in Fig. 4, but the details of the persistence of the plume are somewhat ambiguous in this method of visualization because of strong two-dimensional effects which develop. These are better studied with full-field Kerr cell photographs taken at selected times during the exhaust process. Since the 4" aperture displays these effects on the largest scale, and permits maximum visibility of the interior of the discharge chamber, the bulk of the detailed study of the large-orifice exhaust process is performed on this configuration.

The orifice-discharge chamber configuration used for this portion of the study is shown in Figs. 5 and 6. Note that the outer (positive) electrode exposes only about a 1/2" annular ring to the interior of the chamber. From previous experience, this is known to be a minimum electrode dimension for the establishment of uniform cylindrical discharge sheets. Also note that the pyrex exhaust vessel is now 9" in diameter, permitting greater lateral development of the exhaust pattern before encountering the vessel wall.

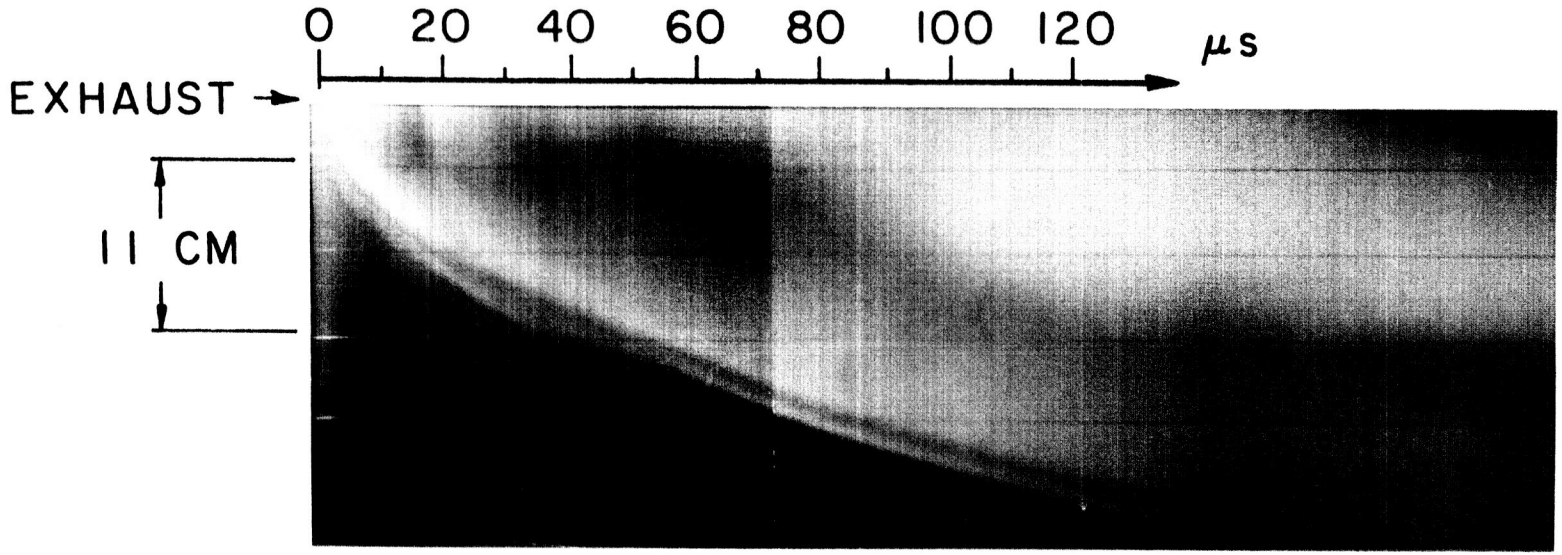

STREAK PHOTOGRAPH OF EXHAUST FROM 5" PINCH DISCHARGE IN 120μ ARGON THROUGH 3/4" DIAMETER ORIFICE

FIGURE 3

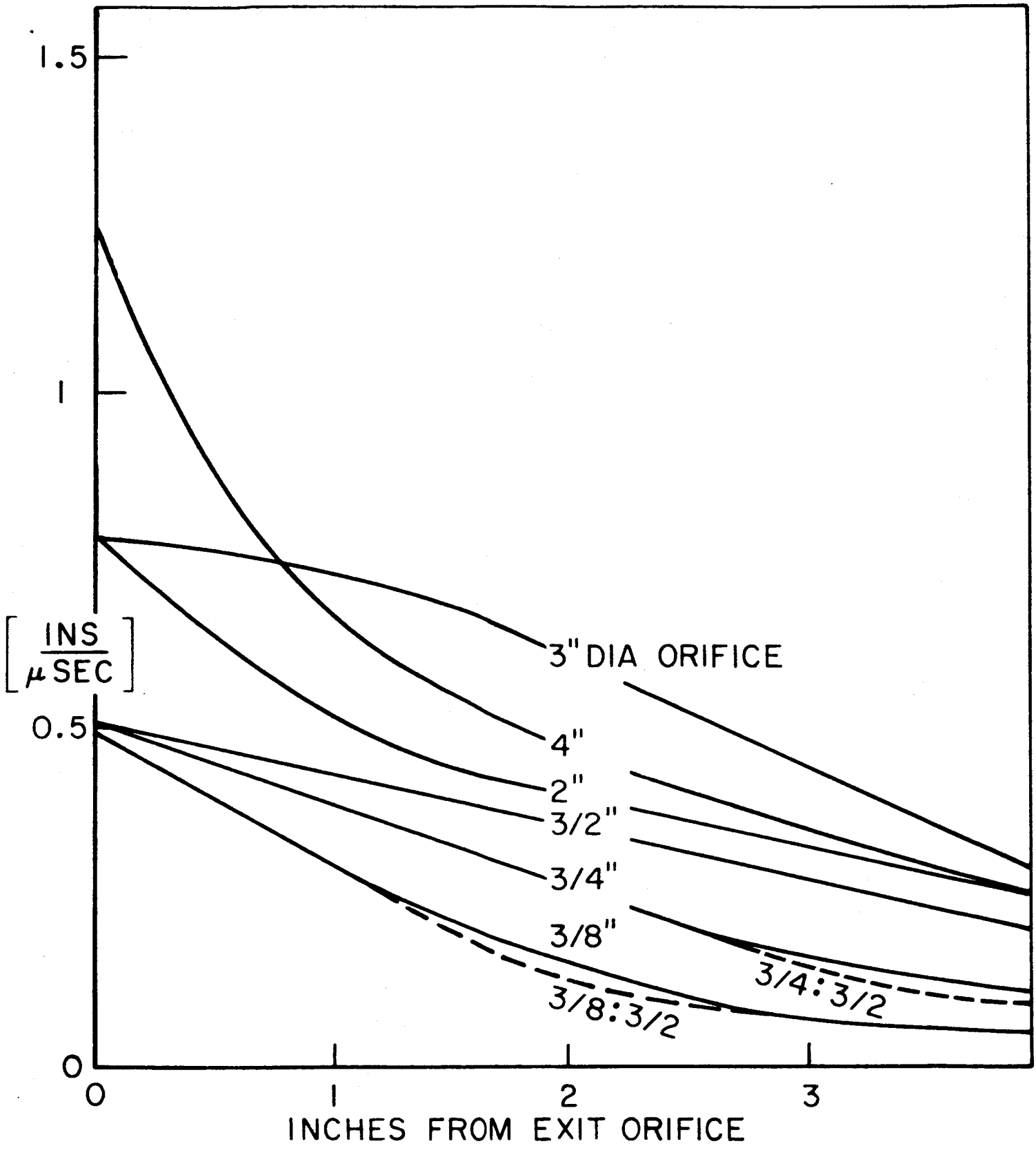

VELOCITY OF EXHAUSTED GAS FROM ORIFICES OF DIFFERENT DIAMETER, IN 120 μ ARGON

FIGURE 4

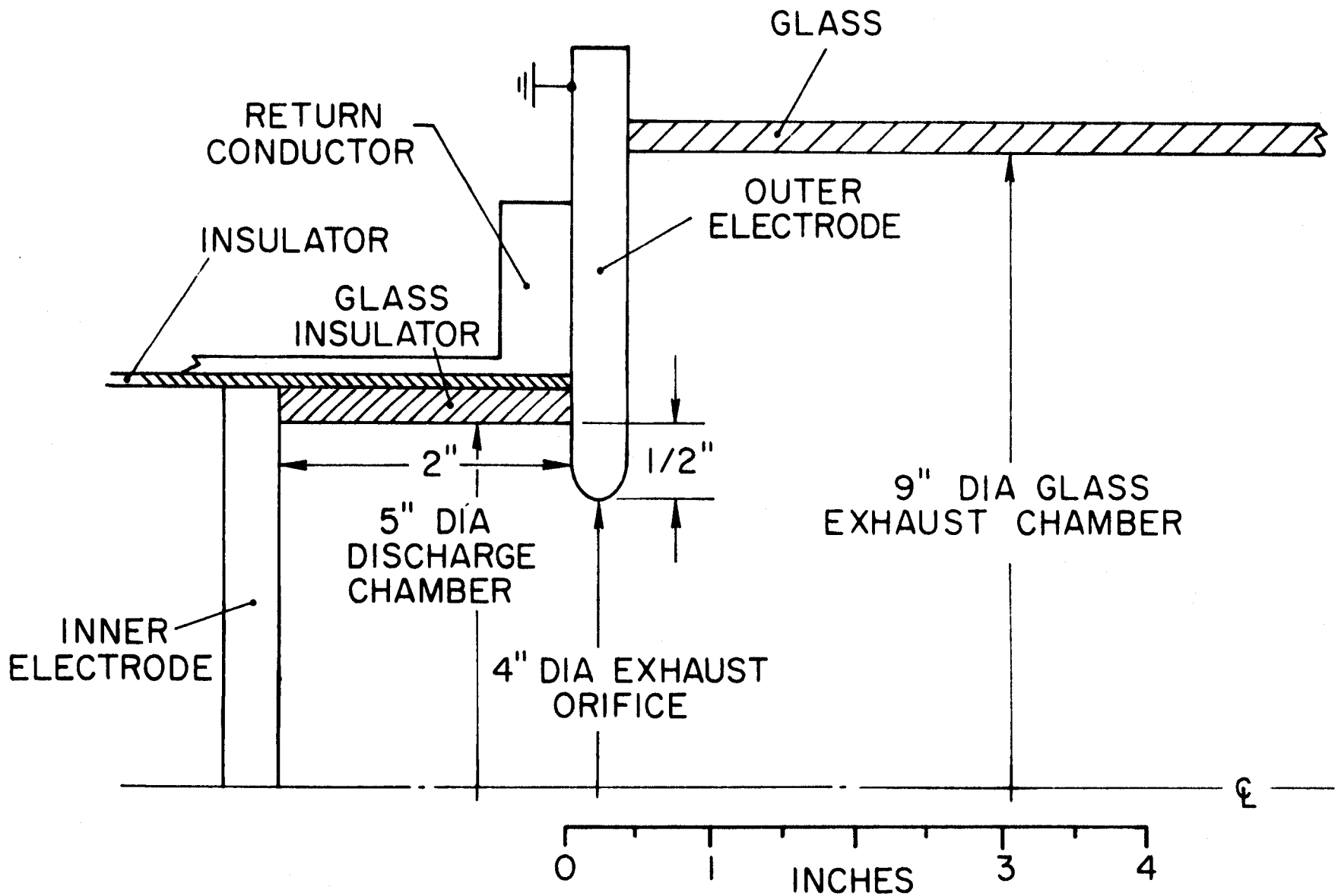

FIGURE 5 DISCHARGE CHAMBER WITH ORIFICE AND EXHAUST CHAMBER (SCHEMATIC)

PINCH DISCHARGE APPARATUS WITH EXHAUST CHAMBER

FIGURE 6

Figure 7 shows a sequence of Kerr cell photographs looking radially into the exhaust vessel at the development of a discharge in 120 μ argon. Figure 8 displays a similar sequence, looking diagonally into the exhaust port, showing additional details of the development of the interior portion of the discharge. Three aspects of the exhaust process are clearly evident in these photographs: 1) The main luminous front originally associated with the interior discharge sheet is observed to diffract outward around the edge of the orifice, and then to propagate axially and radially outward into the exhaust vessel and along the outer face of the electrode. 2) The portion of the cylindrical luminous front inside of the discharge chamber proceeds radially inward essentially undisturbed by the presence of the large aperture in the electrode. It retains an axial and azimuthal symmetry, and a propagation speed that is indistinguishable from those found for discharges in completely closed chambers (14). This remarkable indifference of the pinch process to the removal of a large portion of its electrode has been noted and exploited in earlier work (5). 3) When the interior pinch is completed, the central core of hot plasma thus created first streams axially outward, and subsequently develops some radial growth, presumably after the pinching magnetic field relaxes somewhat. The axial thrust of this luminous column eventually pierces through the envelope of the diffracted luminous front mentioned in 1) above, and sometime thereafter the entire pattern diffuses into invisibility.

Patterns similar to these are observed for discharges at other ambient pressures ranging from 30 μ to 1920 μ of argon, but none of these display the above phenomena so distinctly as the 120 μ discharges. They are of interest, however, in comparing the outward axial speed of ejection of the pinch-heated plasma column with the interior radial speed of the imploding luminous front before the pinch is established. In all cases the ejection speed is found to be a significant fraction of the preceding radial pinching velocity which may imply that much of the random thermal energy resident in the pinch-heated plasma is recoverable as useful streaming motion. Table I summarizes the ratios of these two speeds in various pressure discharges.

TABLE I

Argon Pressure	Radial Sheet Speed, Inside (in/μsec)	Axial Exhaust Speed (in/μsec)	Ratio $\frac{\text{Axial Speed}}{\text{Radial Speed}}$
30 μ	2.20	1.40	0.65
120 μ	1.50	1.20	0.82
480 μ	0.80	0.47	0.60
1920 μ	0.43	0.24	0.54

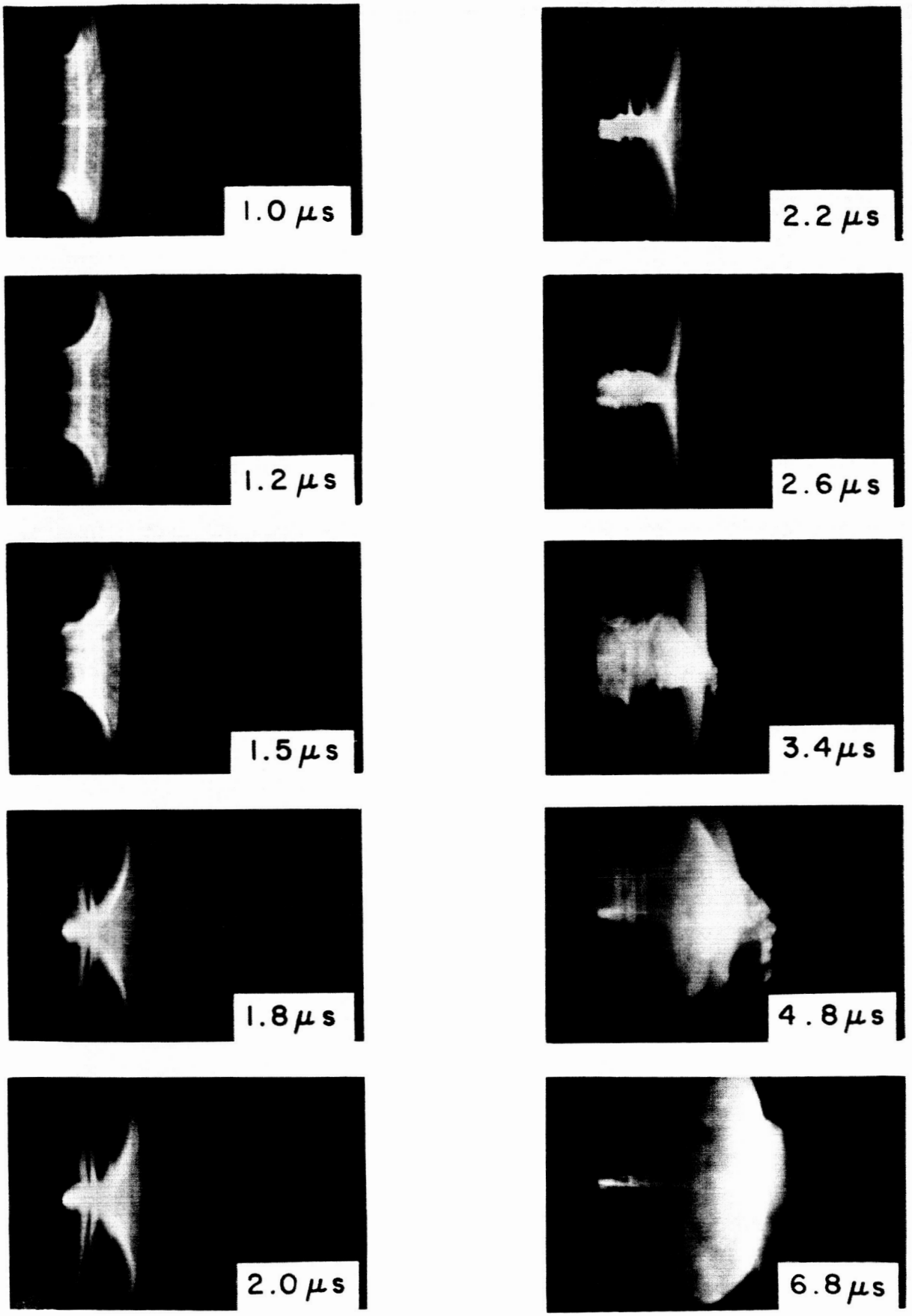

KERR CELL PHOTOGRAPHS OF EXHAUST FROM PINCH DISCHARGE IN 120 μ ARGON

FIGURE 7

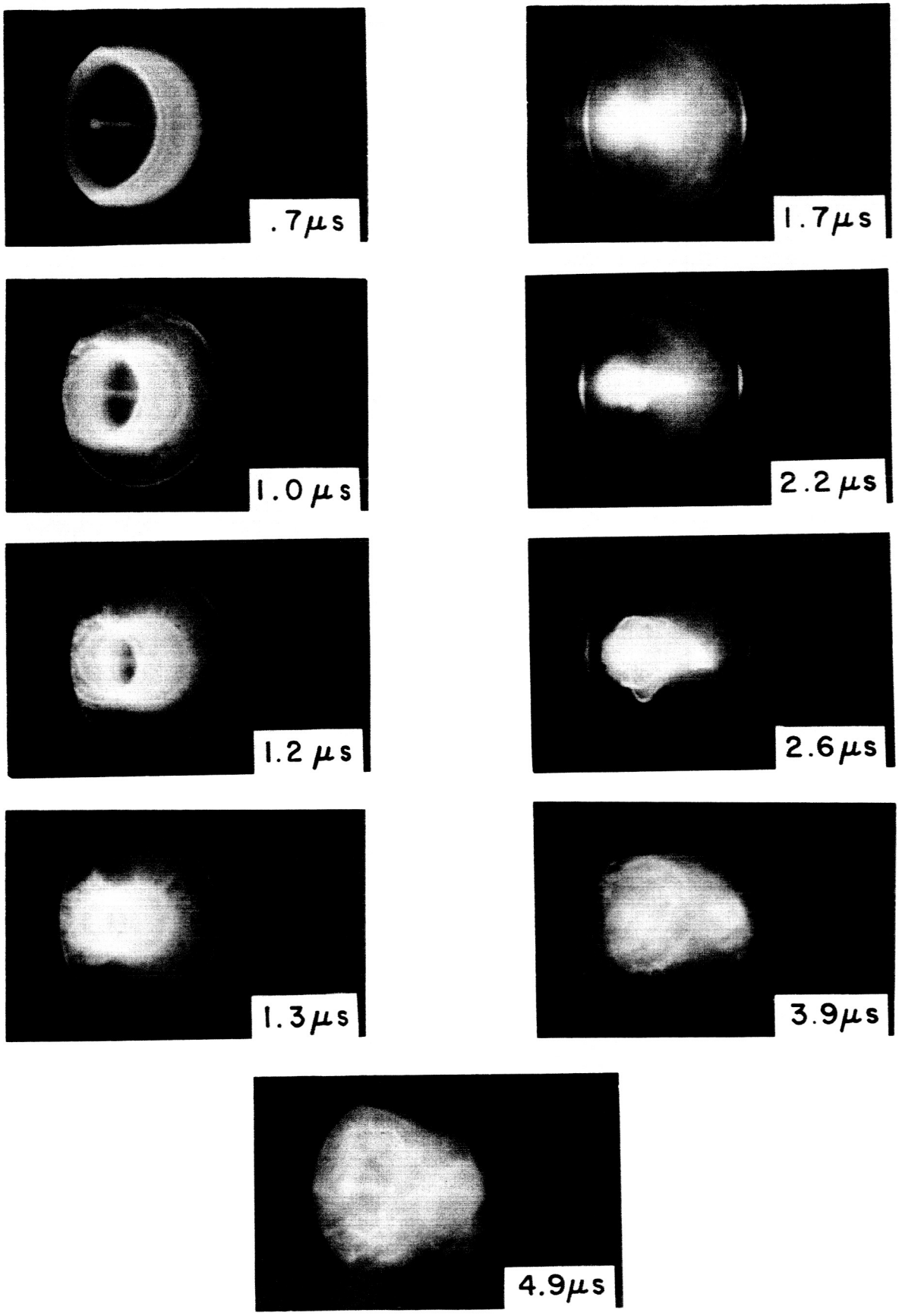

DIAGONAL VIEW OF PINCH DISCHARGE:
120μ ARGON, 4" ORIFICE

FIGURE 8

One strongly suspects that the luminous front which diffracts out of the orifice is associated with a current-carrying region, much like the luminous fronts and related current sheets inside the discharge chamber (14). Indeed, one expects that it is the self-magnetic field trapped behind this diffracting front which is driving it outward. To confirm this concept, a series of magnetic probe surveys were performed to map the development of the interior and exterior magnetic fields, and from them to deduce the current density distributions inside the chamber and within the exhaust plume. The magnetic probe employed was constructed of 3 turns of #32 formvar wire, 0.076" in diameter, enclosed in a 0.15" pyrex tube which projected axially into the discharge at the desired radii (cf. Fig. 9). The signals from the probe were passively integrated on the face of a Tektronix 555 oscilloscope, and displayed and photographed thereon at 0.5 μsec/cm. Typical current profiles deduced from a series of such records are shown in Figs. 10-14. The data here are presented in the form of contours of total current enclosed within the radius of the field point, or equivalently, contours of the product of the local magnetic induction field and the radius. Arrowheads indicate the direction of local electron current. The location of the diffracted luminous front at the corresponding time is superimposed as a dotted curve. It is seen that these luminous fronts are indeed associated with regions of high current density and correspondingly high magnetic body forces, acting to drive them away from the orifice.

The distributions of current density and magnetic field within the chamber, like the luminous front patterns, are essentially the same as those found in a corresponding closed chamber experiment. No serious distortion of the profiles is found until the probe is withdrawn into the geometrical shadow of the aperture.

At late times, the current density patterns in the chamber and plume become badly distorted by the ringing of the external circuit and the "crow-bar" discharges attendant the external current reversals (14). While these produce certain curious effects, such as the complete detachment of a current "vortex" within the plume, and a severe recirculation pattern on the outer electrode surface, they are not the main interest of the present study.

In order to remove these complications from the current distributions, the discharge apparatus was modified to accept the transmission line capacitor arrangement described in detail in the following section. With this modification it was possible to apply a rectangular current pulse of 200,000 amps persisting for about 5 μsec before reversal. Figure 15 shows a photograph of this arrangement, and Fig. 16 compares the current waveform derived from it with the typical ringing discharge supplied by the usual lumped bank.

VIEW OF MAGNETIC PROBE IN DISCHARGE CHAMBER

FIGURE 9

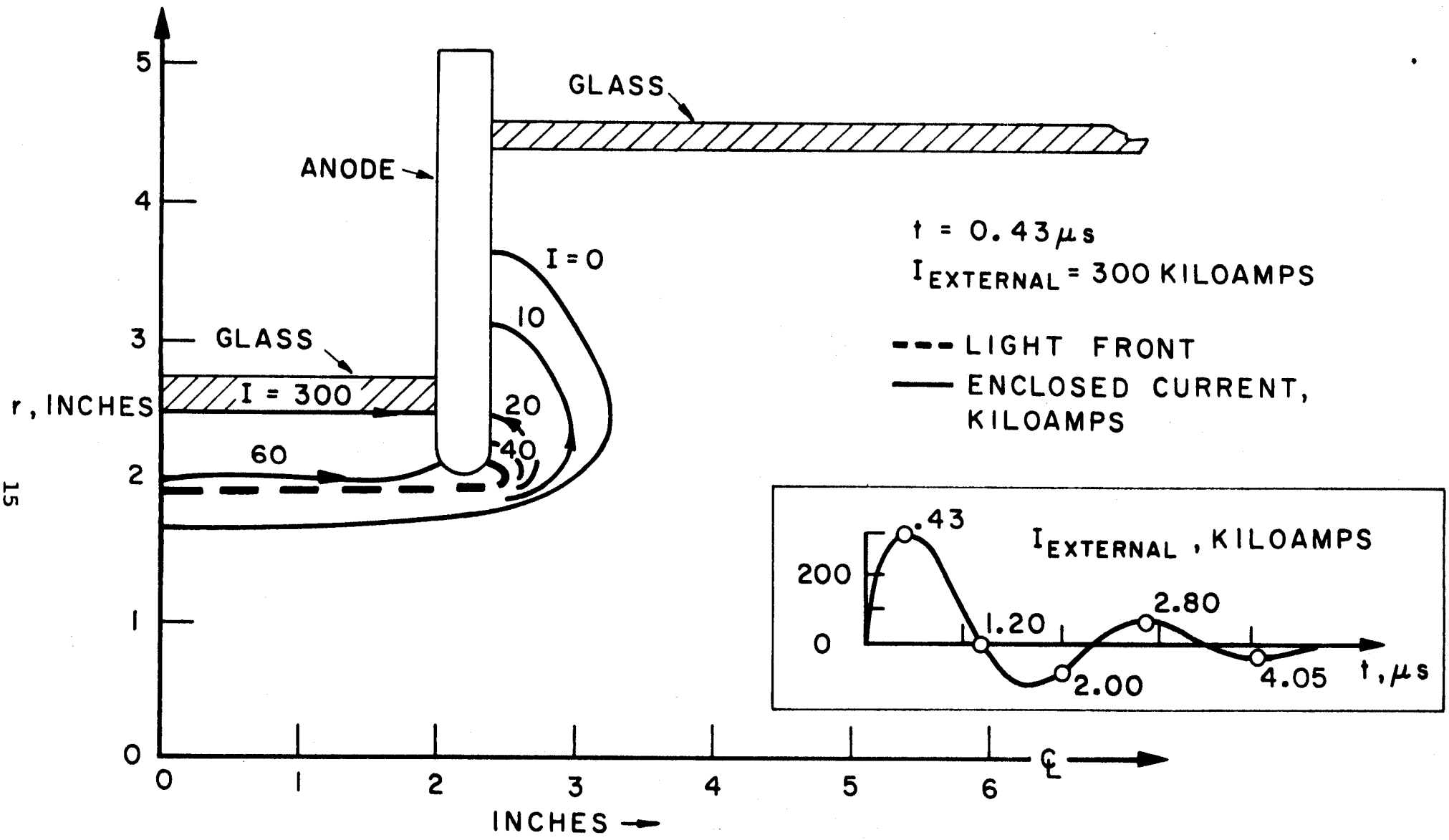

FIGURE 10

CURRENT PROFILES
120 μ ARGON, 4" ORIFICE

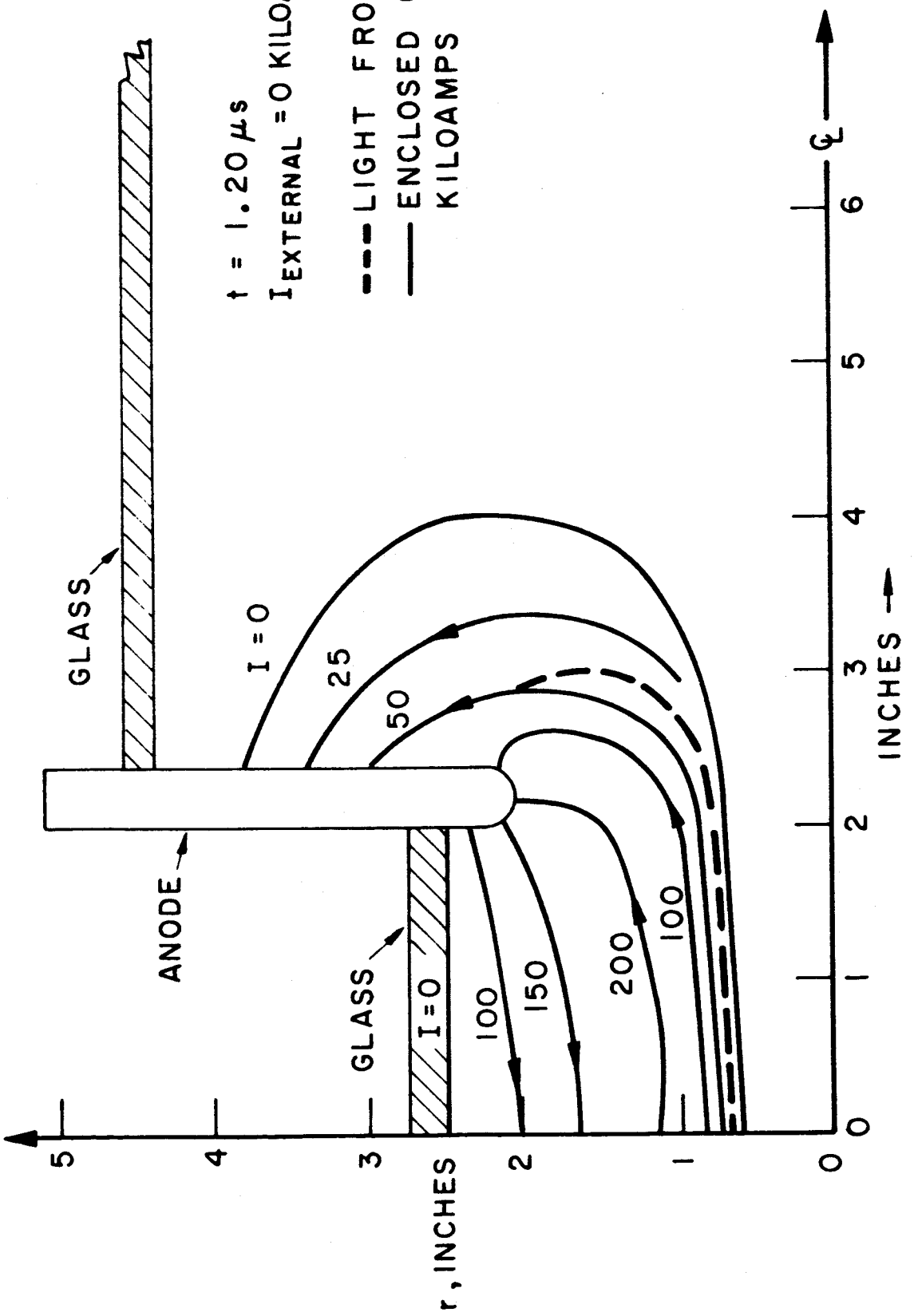

CURRENT PROFILES
120 μ ARGON, 4" ORIFICE

FIGURE 11

P-25-JPR 4005-64

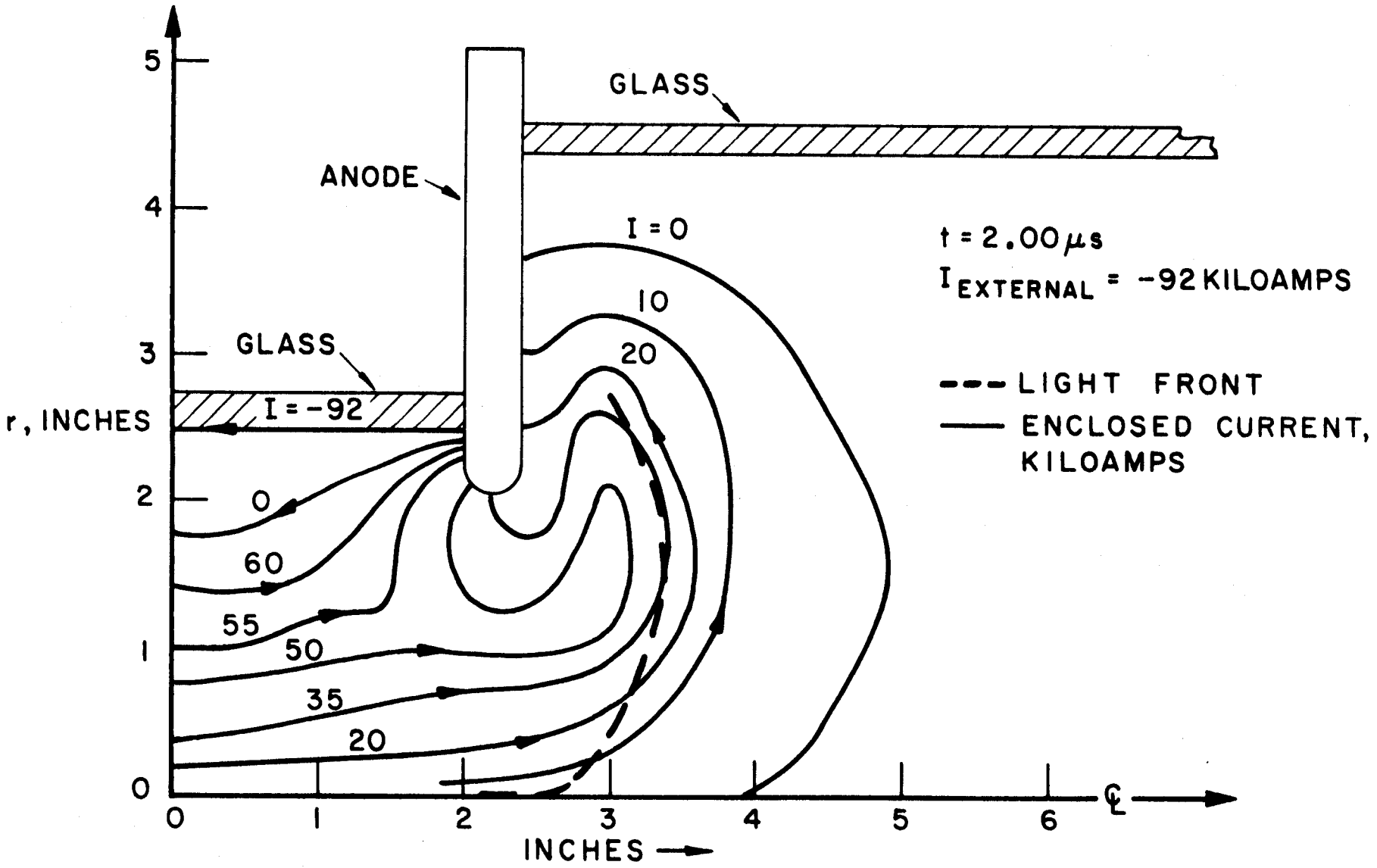

FIGURE 12

CURRENT PROFILES
120 μ ARGON, 4" ORIFICE

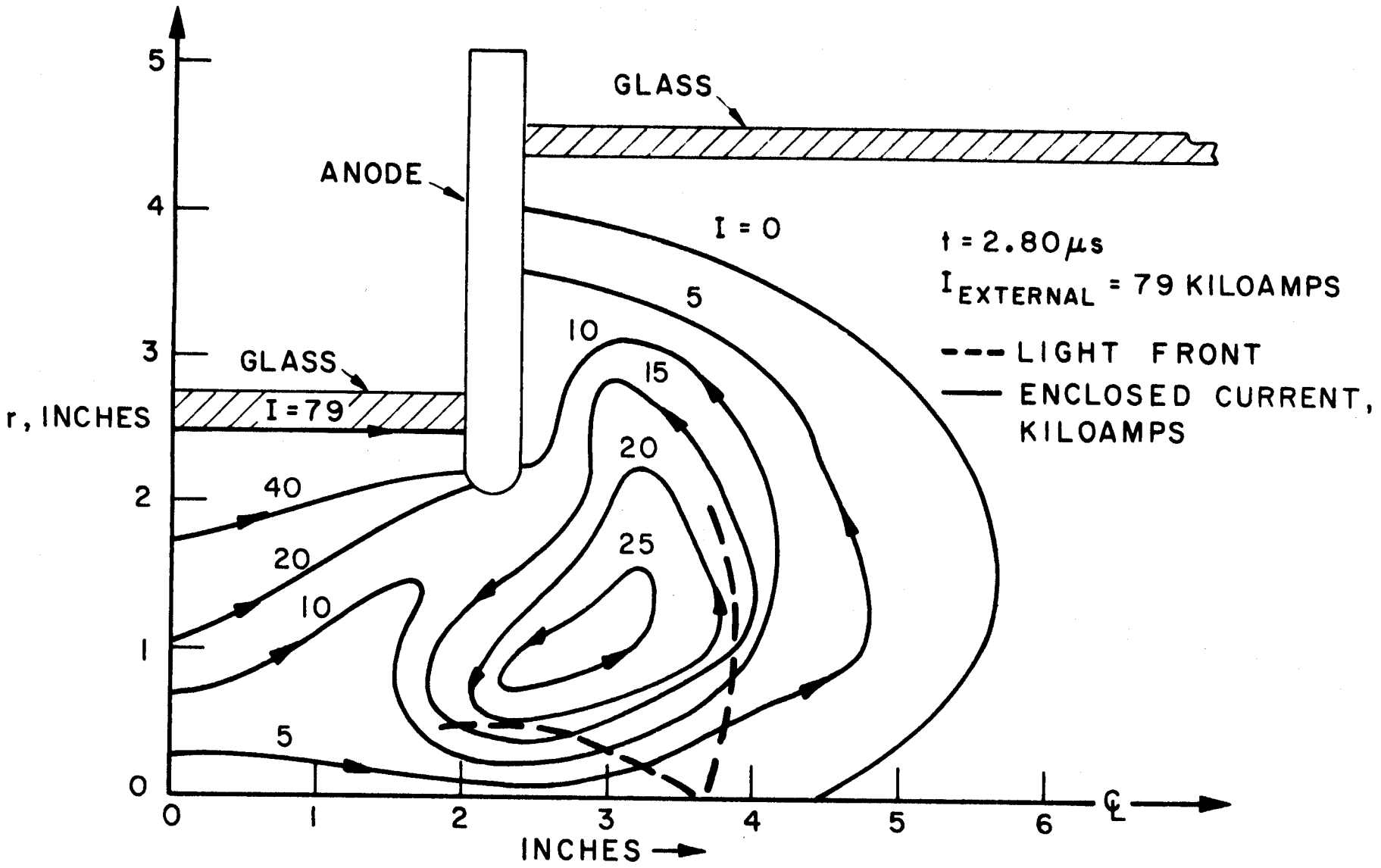

FIGURE 13

CURRENT PROFILES
120 μ ARGON, 4" ORIFICE

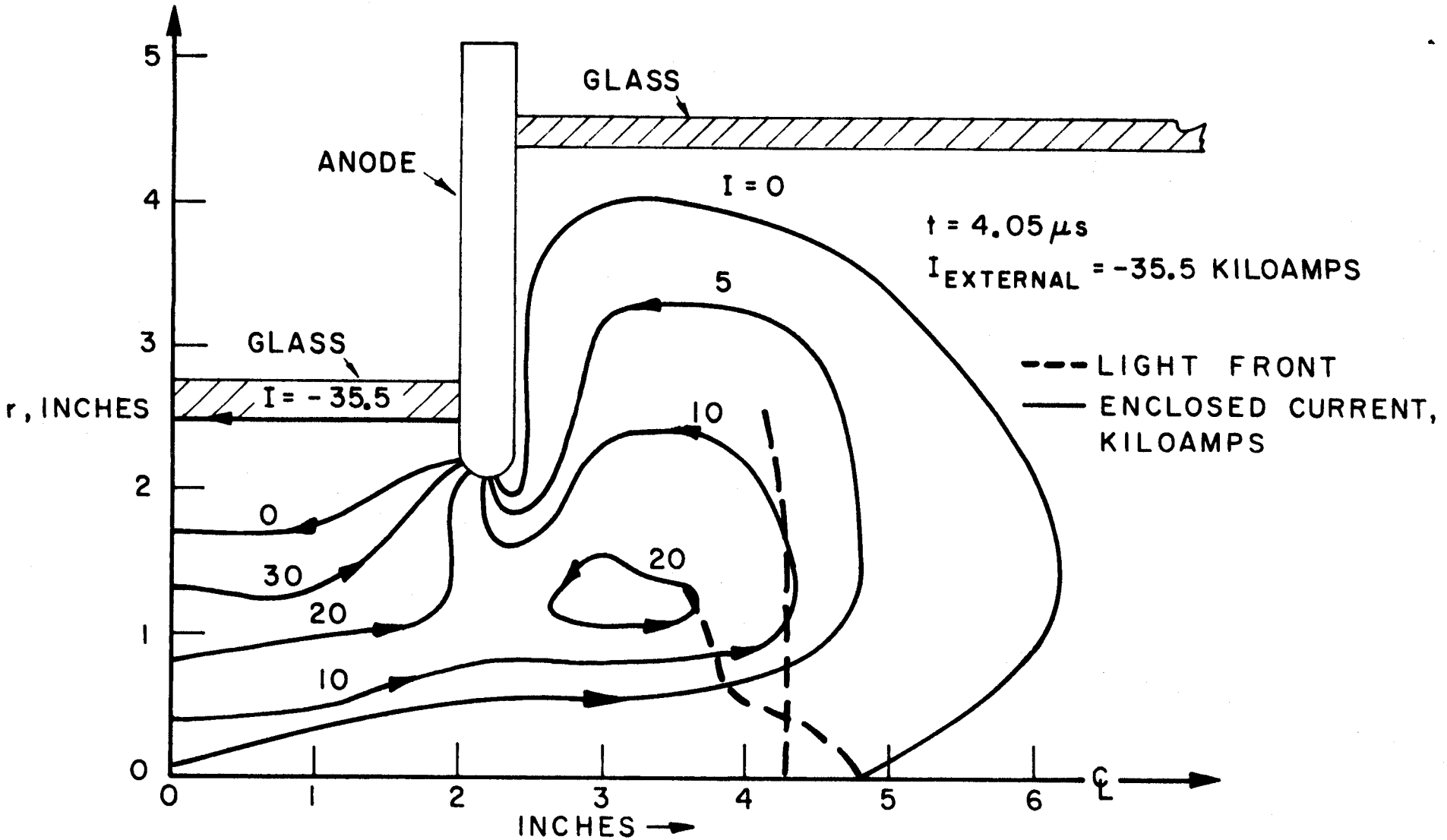

FIGURE 14

CURRENT PROFILES
120 μ ARGON, 4" ORIFICE

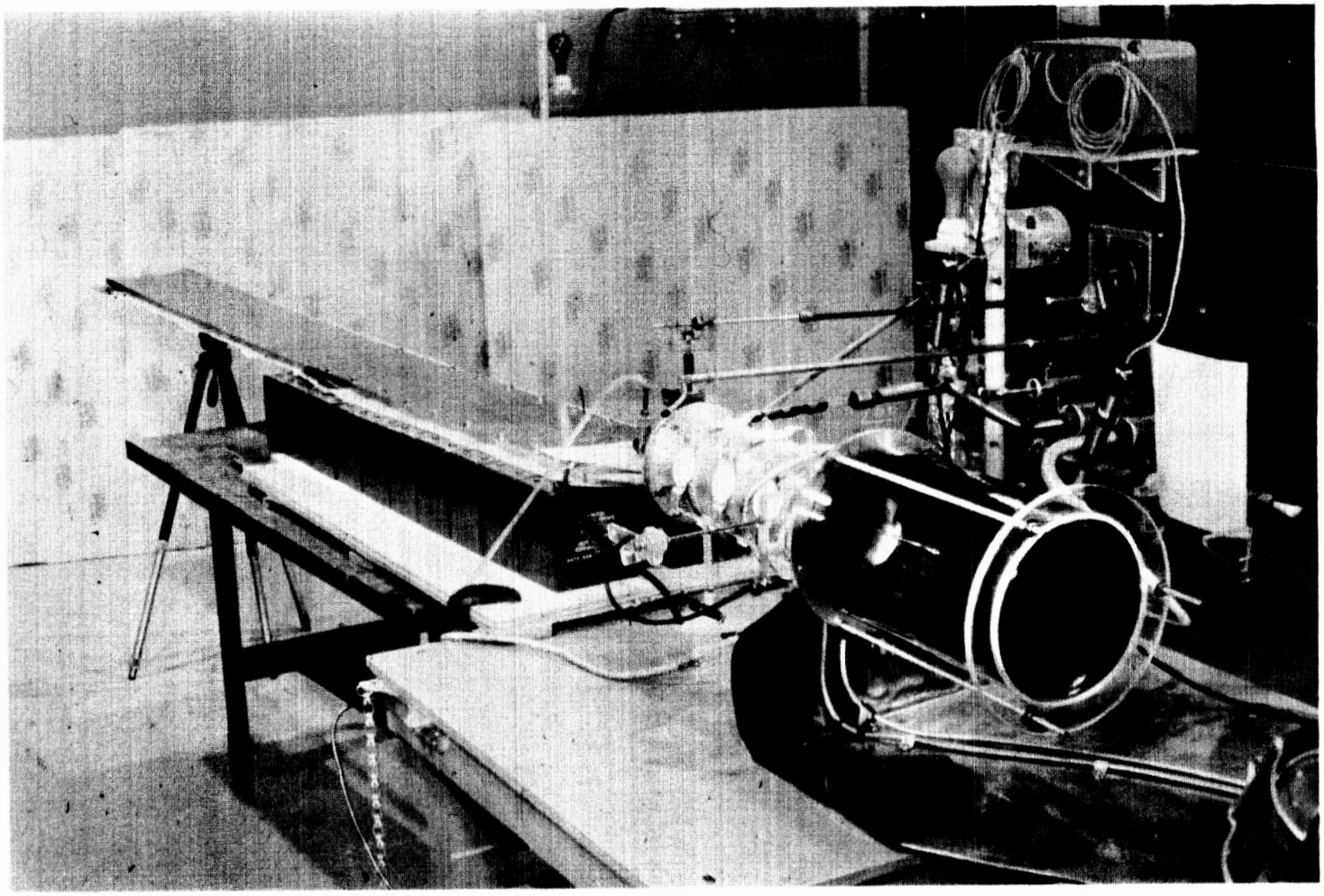

VIEW OF PINCH EXHAUST APPARATUS WITH PULSE LINE

FIGURE 15

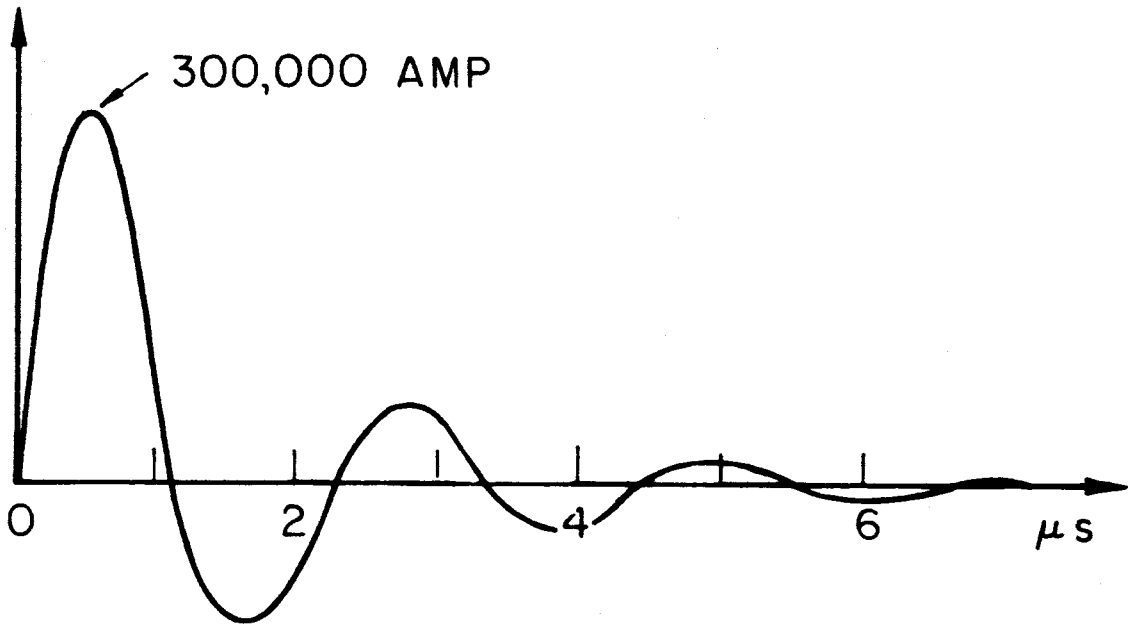

PARALLEL CAPACITOR BANK

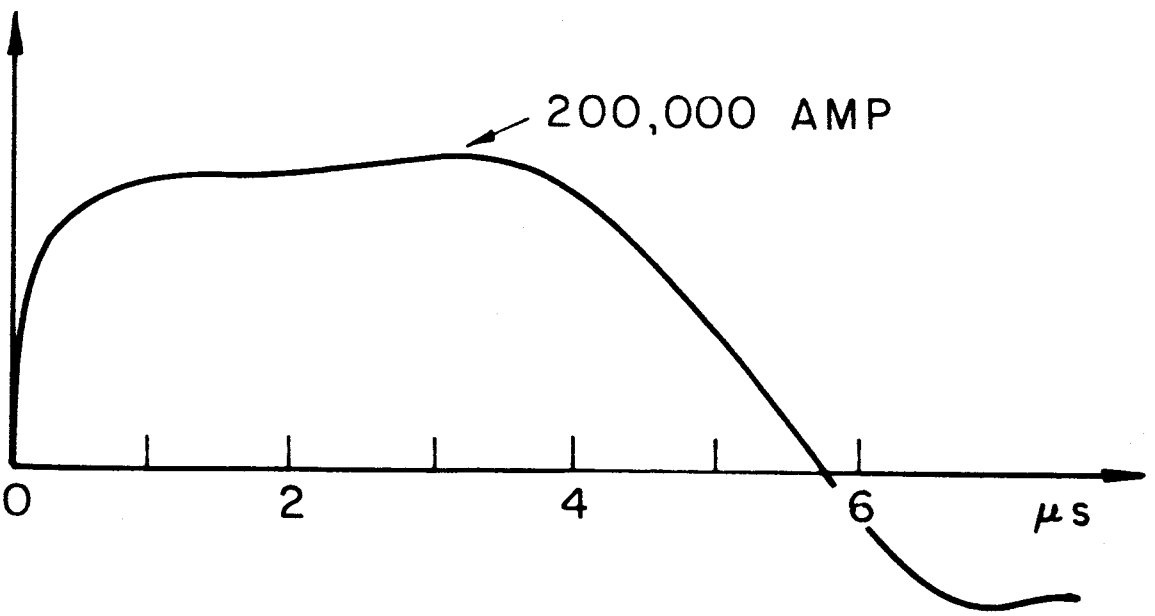

PULSE FORMING NETWORK

CURRENT WAVEFORMS
FOR PINCH DISCHARGE

FIGURE 16

Figures 17-22 show the current density distributions obtained in the plume and within the chamber for a 120 μ argon discharge driven by the rectangular pulse. Again the interior patterns are essentially the same as for the closed chamber discharges driven by the same circuit. The plume patterns now do not develop the vortex features found in the ringing discharge until after the end of the rectangular pulse, confirming our suspicion that these arise primarily from external circuit current reversal. Some distortion of the patterns is found near the edge of the orifice, and some near the wall of the exhaust vessel, perhaps implying a gasdynamic influence on the current trajectories there.

The luminous phenomena occurring in the rectangular pulse discharges are observed to be qualitatively similar to those seen in the ringing discharge, but the absolute velocities of the various fronts are significantly higher. Figure 23 shows a few Kerr cell photographs of these luminous patterns, and Fig. 24 compares the radial trajectory of the interior front with the axial trajectories of the diffracted front and the thermal column. Note that now the axial expansion of the pinch column begins with speeds substantially higher than that of the foregoing interior radial motion, again indicative of significant recovery of the thermal energy deposited in this column.

In passing, it may be relevant to examine the essentially transient nature of the entire ejection process. While the radial and axial outward propagation of the diffracted front seems reasonable in view of the appropriate magnetic body forces supplied by the field trapped behind it, there are several well-known situations, at least superficially comparable, where such propagation does not occur. For example, in the presently popular high impulse arcjets, a radial current zone of not greatly lower density remains attached to the edge of the anode orifice. Similarly, experiments with pseudo-steady flow coaxial guns show that the transient propagation of the current sheet down the barrel terminates with the current zone stabilizing at the barrel exit rather than detaching or billowing out into the exhaust tank. The criterion which distinguishes those two behaviors is at present not clear. Further experiments with longer duration driving current pulses and larger exhaust vessels may possibly reveal an eventual stabilization of the exhaust pattern. These are currently under consideration.

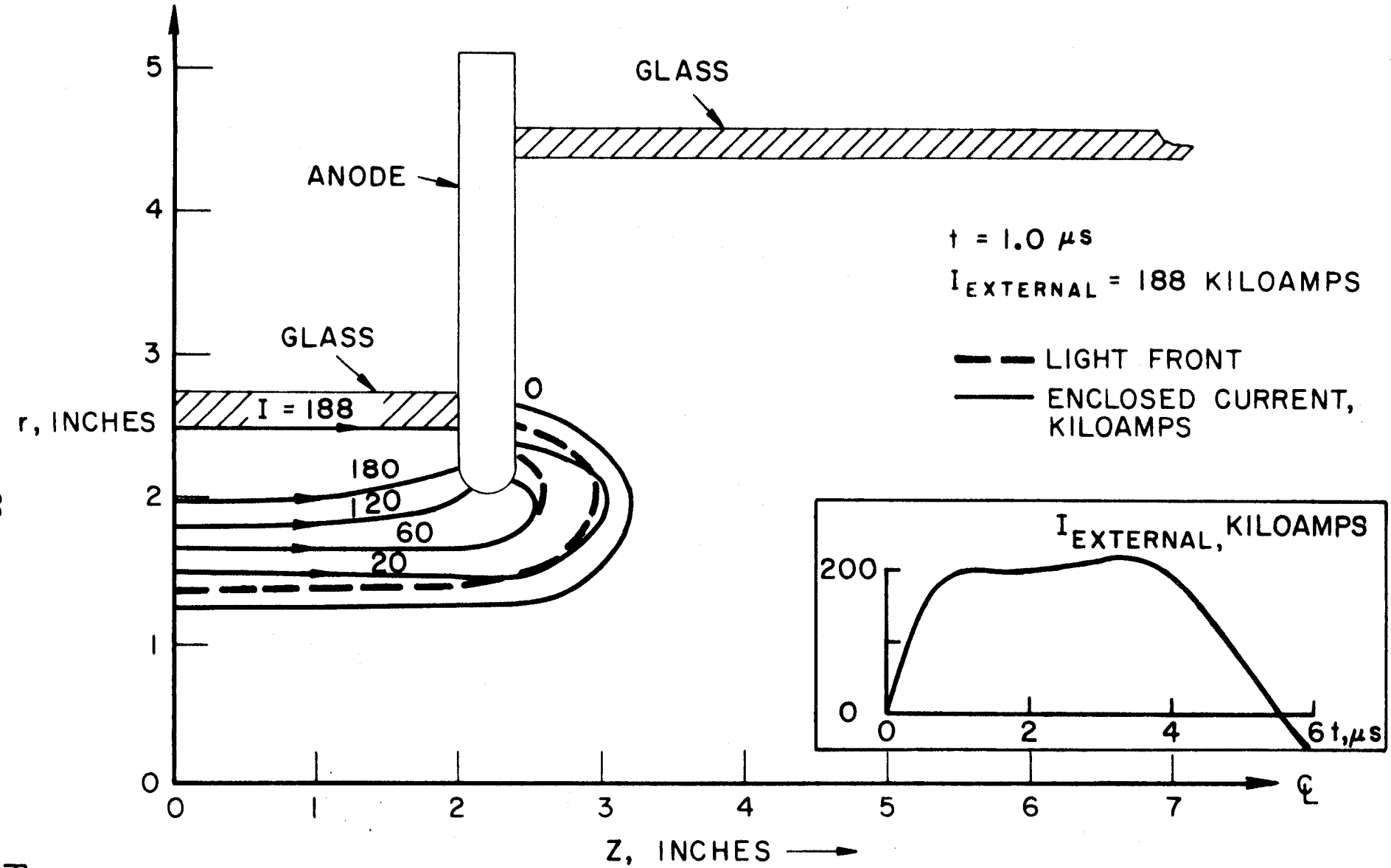

FIGURE 17

CURRENT PROFILES
120 μ ARGON, 4" ORIFICE

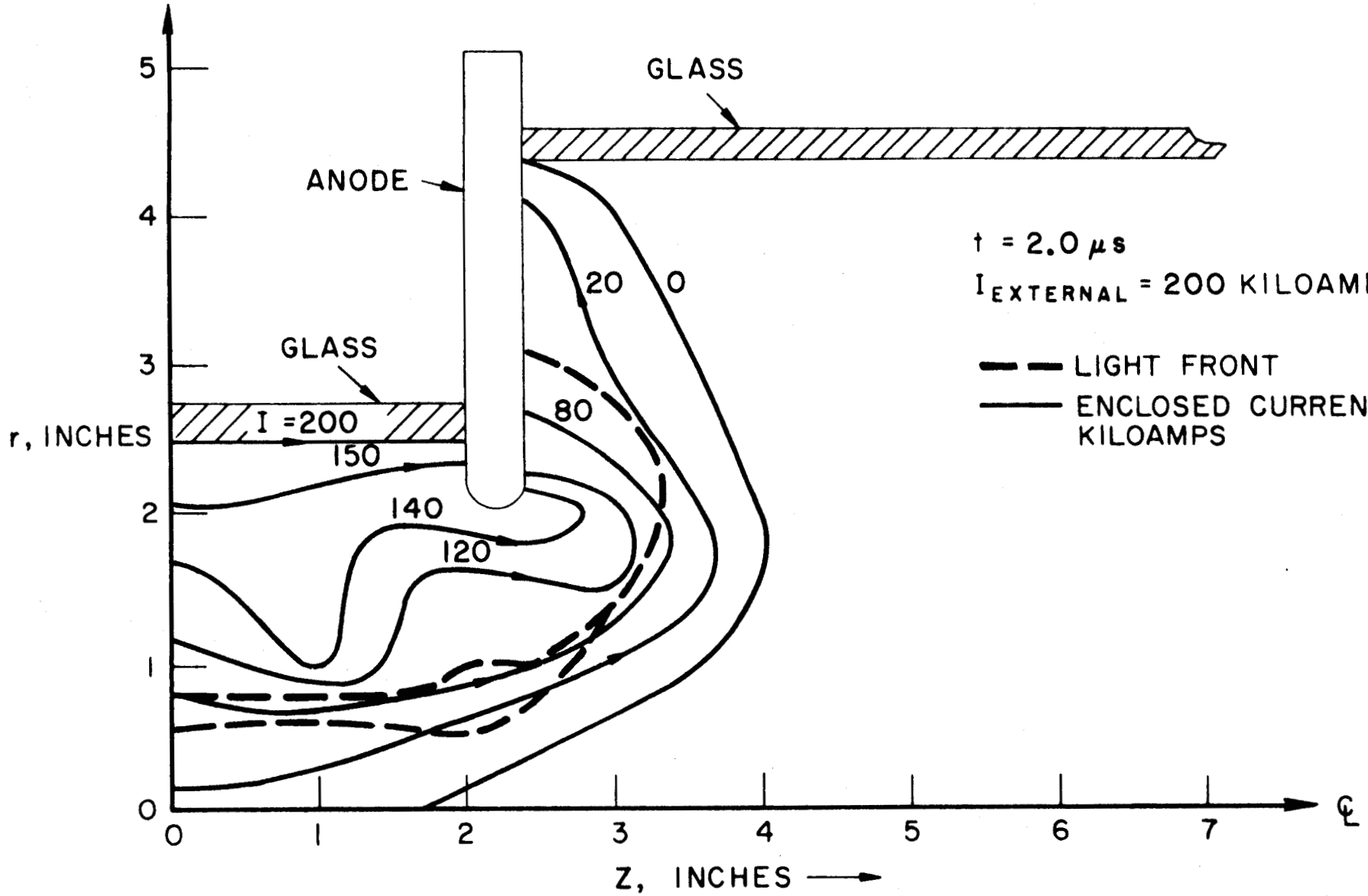

FIGURE 18

CURRENT PROFILES
120 μ ARGON, 4" ORIFICE

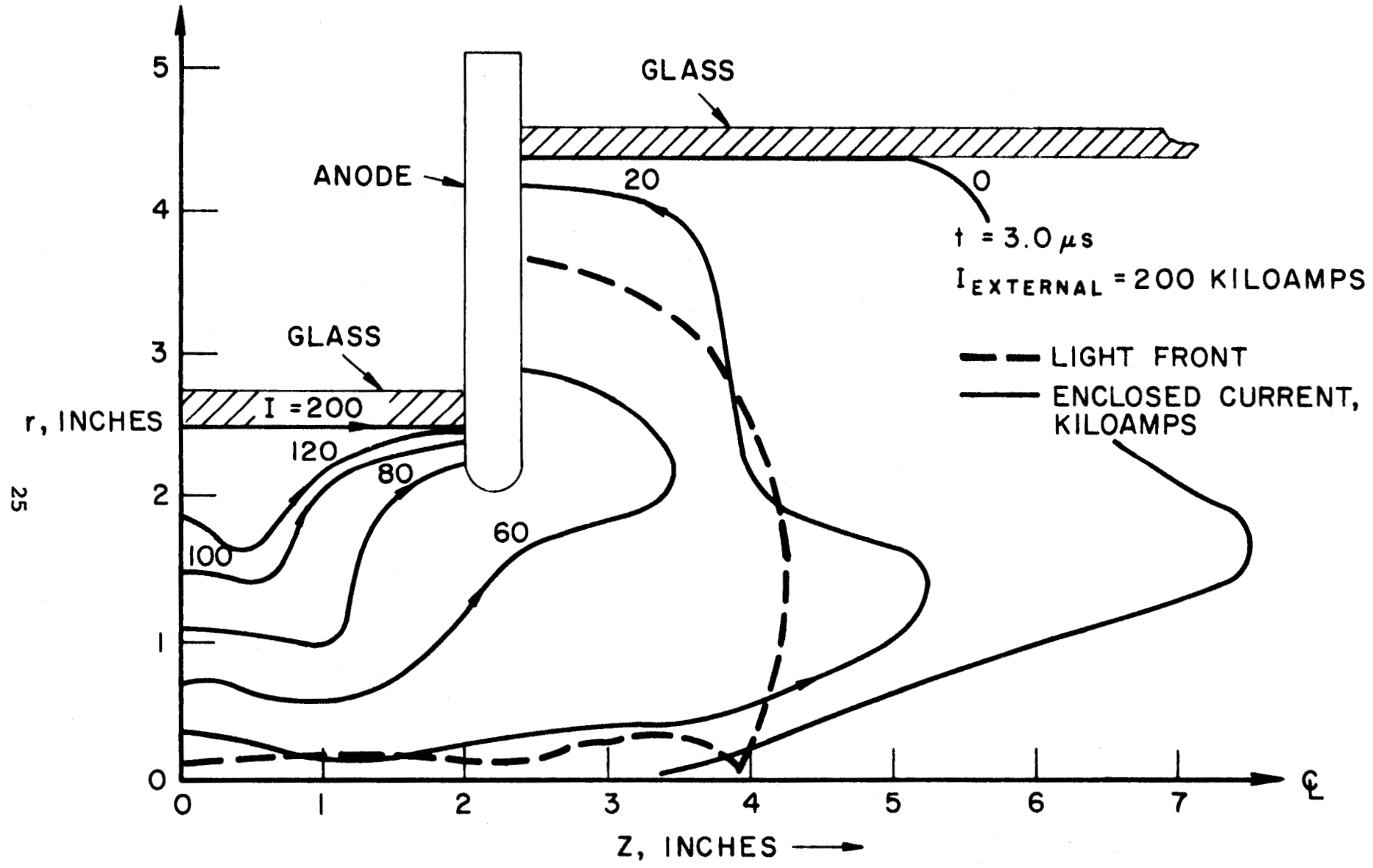

FIGURE 19

CURRENT PROFILES
120 μ ARGON, 4" ORIFICE

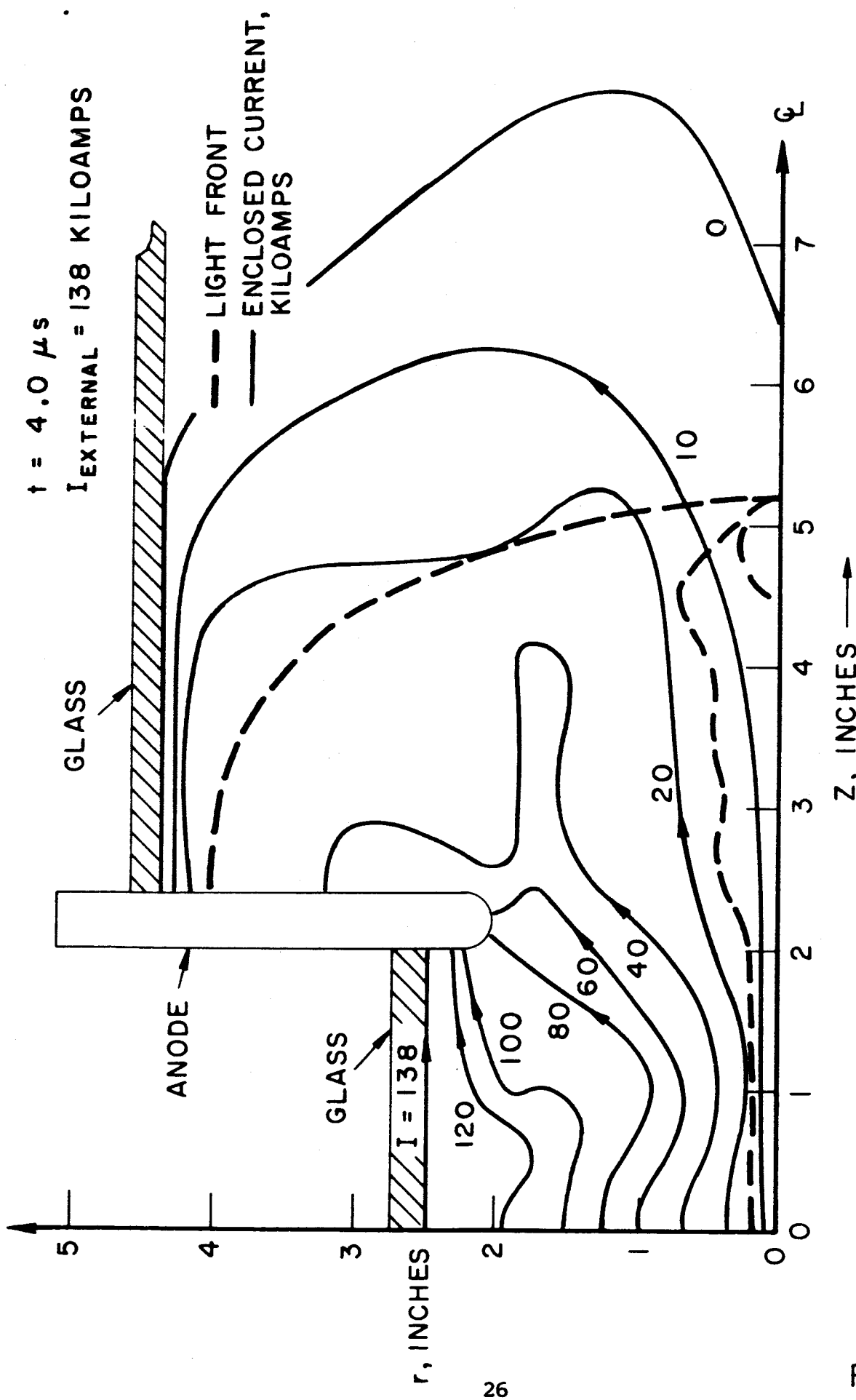

CURRENT PROFILES
120 μ ARGON, 4" ORIFICE

FIGURE 20

AP 25. JPR 4013-65

AP25-JPR 4014-65

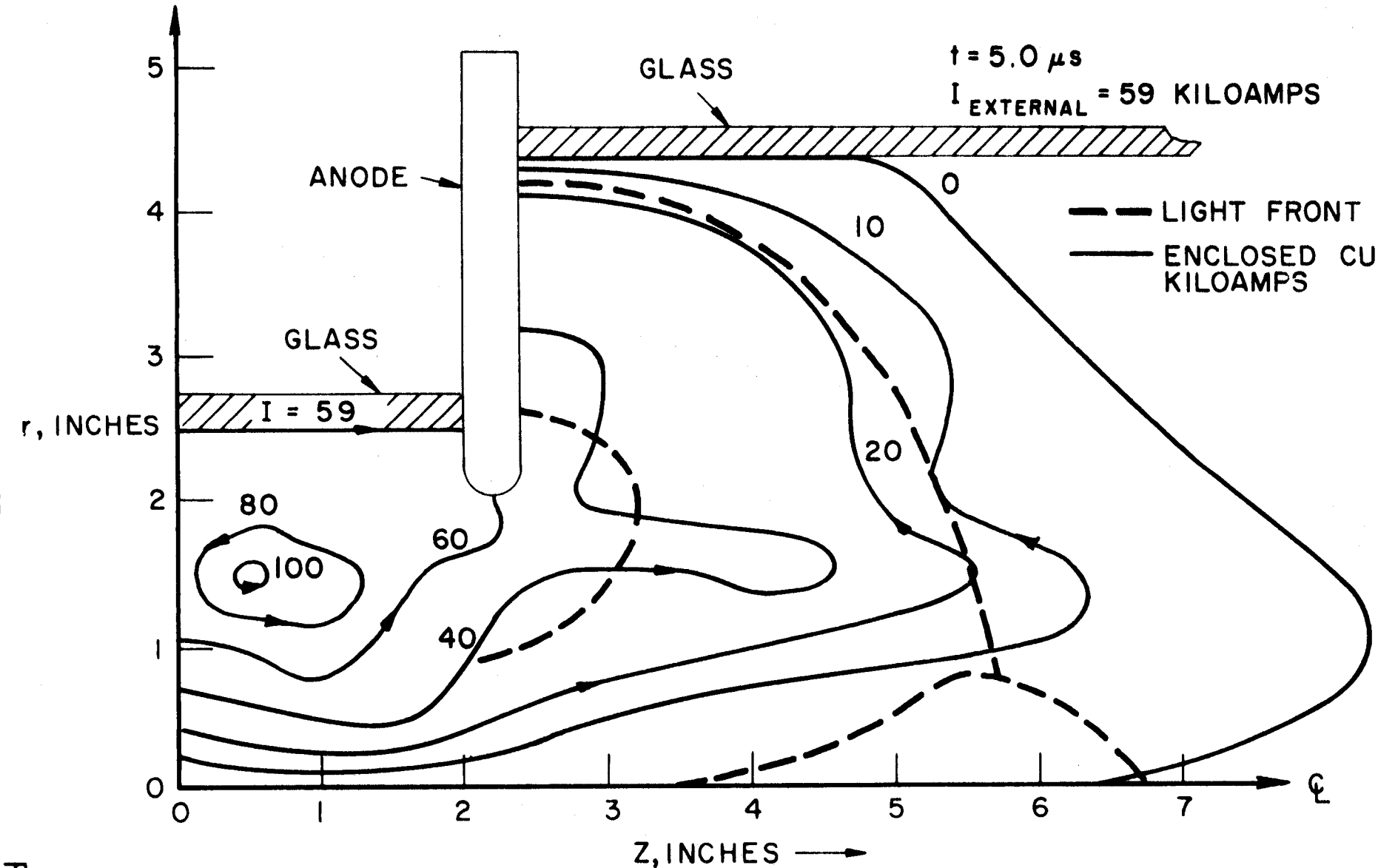

CURRENT PROFILES
120 μ ARGON, 4" ORIFICE

FIGURE 21

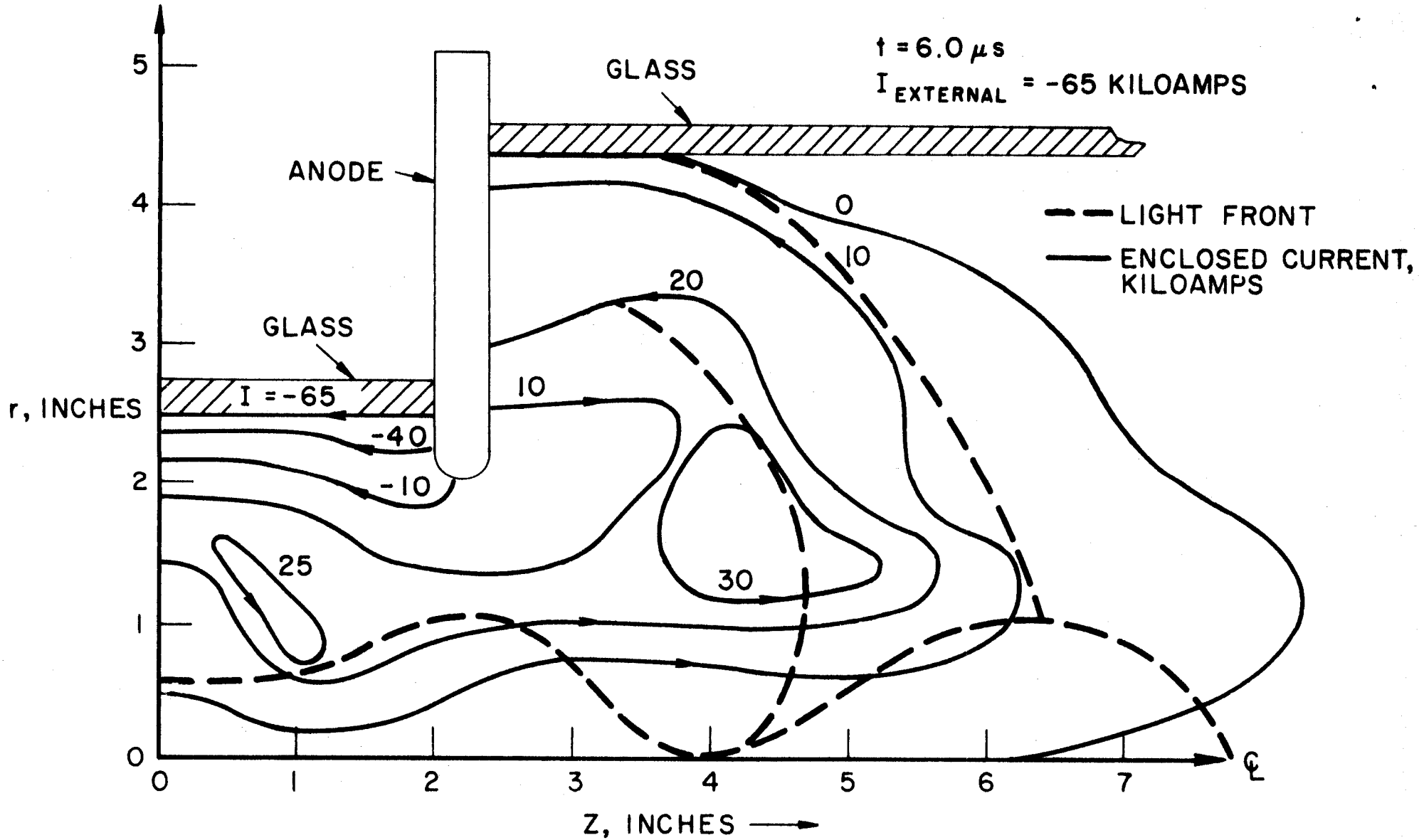

FIGURE 22

CURRENT PROFILES
120 μ ARGON, 4" ORIFICE

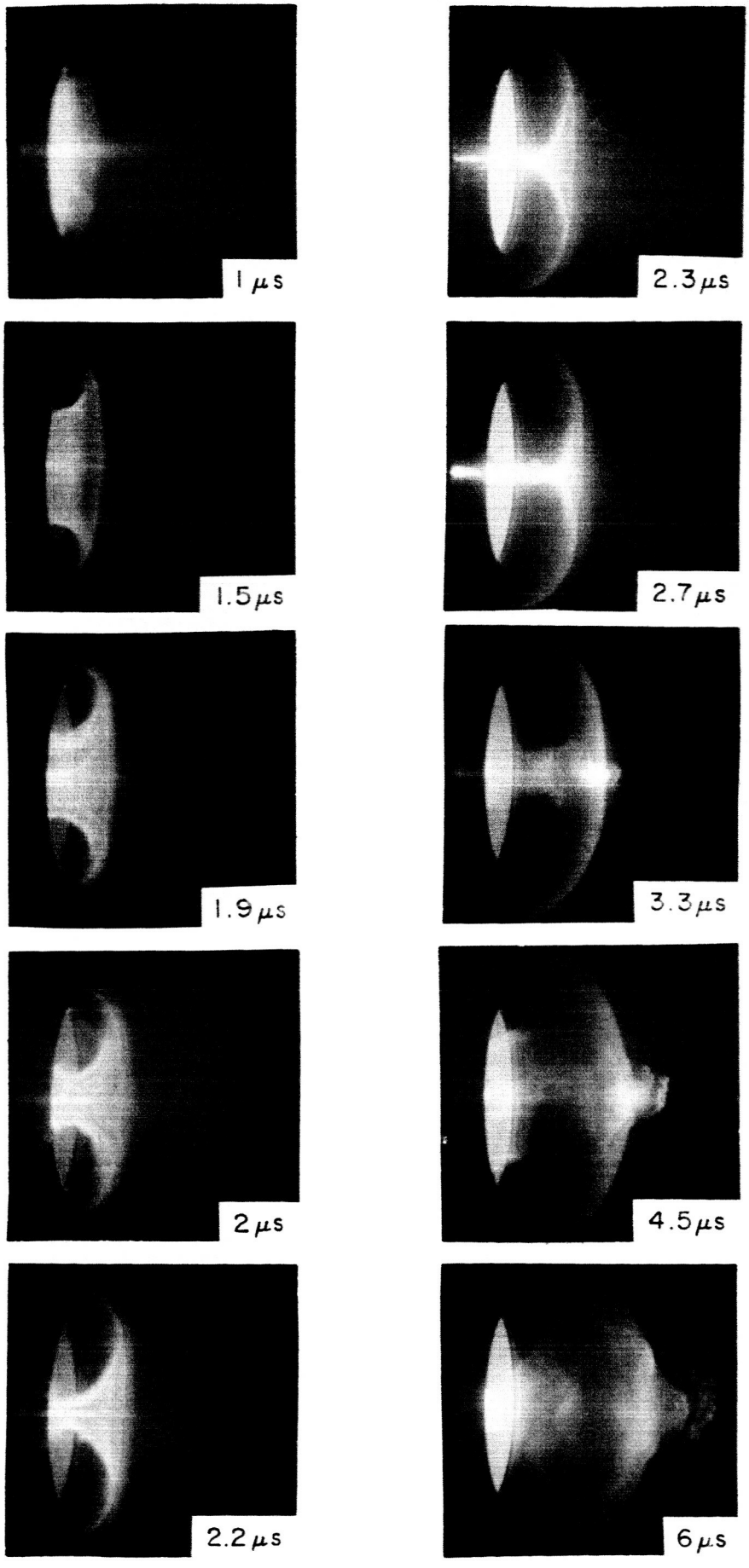

KERR CELL PHOTOGRAPHS OF EXHAUST FROM CONSTANT CURRENT PINCH IN 120 μ ARGON

FIGURE 23

AP25-P15-65

AP25-JPR-4009-65

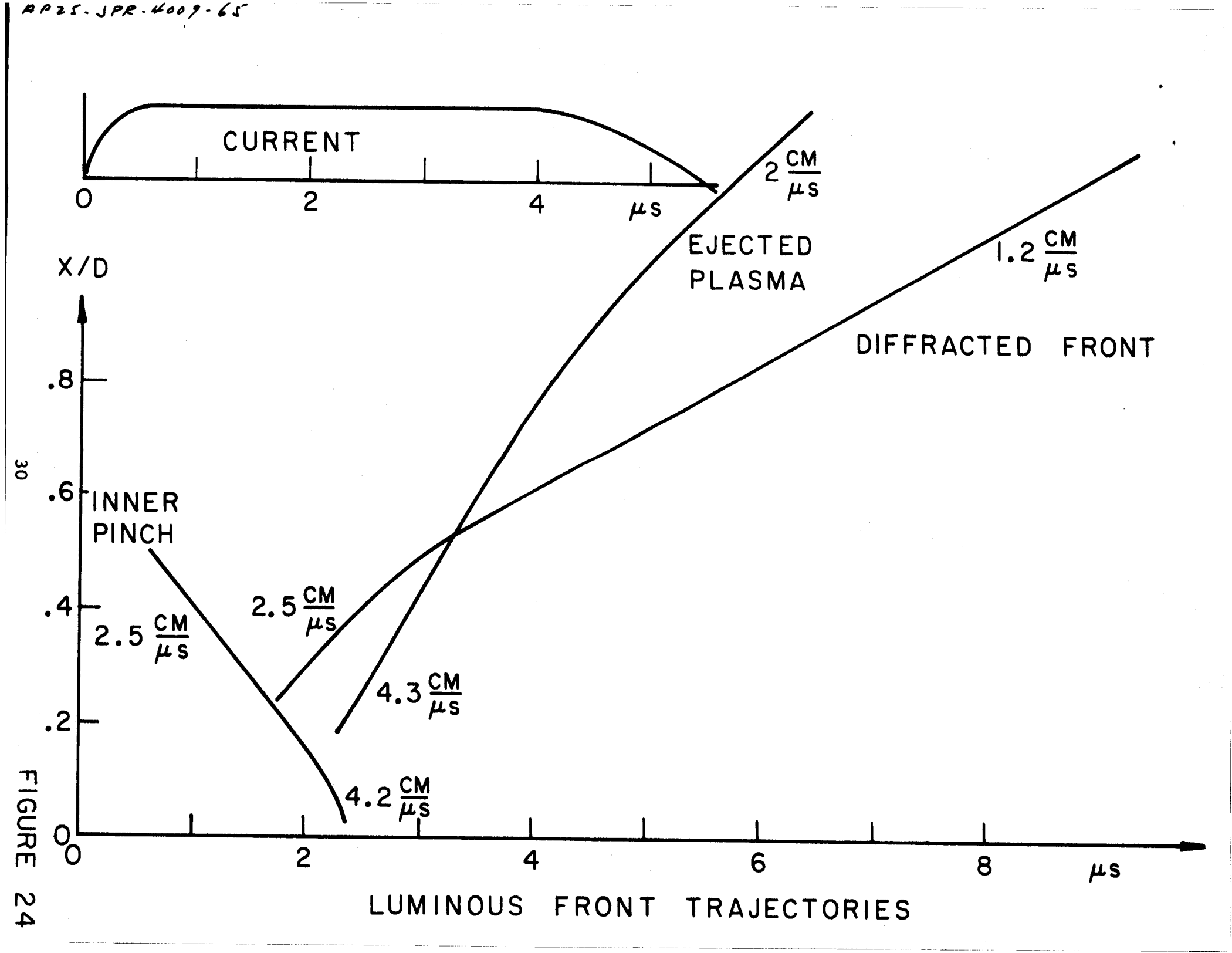

LUMINOUS FRONT TRAJECTORIES

FIGURE 24

III. PULSE-FORMING NETWORK DISCHARGE STUDIES (Black, Jahn)

In the course of the earlier experimental and analytical studies of the large-radius pinch discharges it became increasingly evident that considerable advantage could be gained by programming the discharge circuit to deliver specific current waveforms, rather than simply accepting the typical sinusoidal oscillations of an underdamped lumped capacitance. The disadvantage of the latter mode of operation is associated with the secondary "crow-bar" discharges which arise at the periphery of the chamber at the time of each reversal of the external current (5,14). First, these secondary discharges interfere with the interior diagnostic measurements and complicate the theoretical representation of the processes. Second, they substantially reduce the attainable gas accelerations, since the primary current pulse is effectively uncoupled from the driving circuit at the time of secondary breakdown.

The design and construction of a pulse-forming network for such applications is far from a trivial project, however. For the very low load impedances involved here, and with the severe requirements on current rise time and amplitude, the usual capacitance and inductance components available are far from adequate. Instead, it was found necessary to place special orders for very low inductance capacitor units, and to fabricate a transmission line in the form of parallel conducting plates, separated by a small thickness of dielectric.

The present form of the device is shown in the schematic drawings of Figs. 25 and 26 and the photograph of Fig. 27. Two ten-foot long inductance wings extend radially from an 8" diameter pinch chamber and coaxial gas-triggered switch of our usual design (15). Each wing has 20 stations and each station can hold 0, 1, or 2 of our (nominal) 2.5 microfarad 10,000 volt Aerovox capacitor units. In typical operation, one man can set up any desired configuration of capacitors in about ten minutes.

Even using only the 25 capacitors now on hand, the number of distinct waveforms attainable by various combinations of these units, is astronomical. To aid us in the selection of capacitor arrangements, a computer program has been generated to explore the current waveforms obtainable by permutation of the capacitors. Referring to the sketch on the following page, which represents the two halves of the pulse-forming network connected across the discharge,

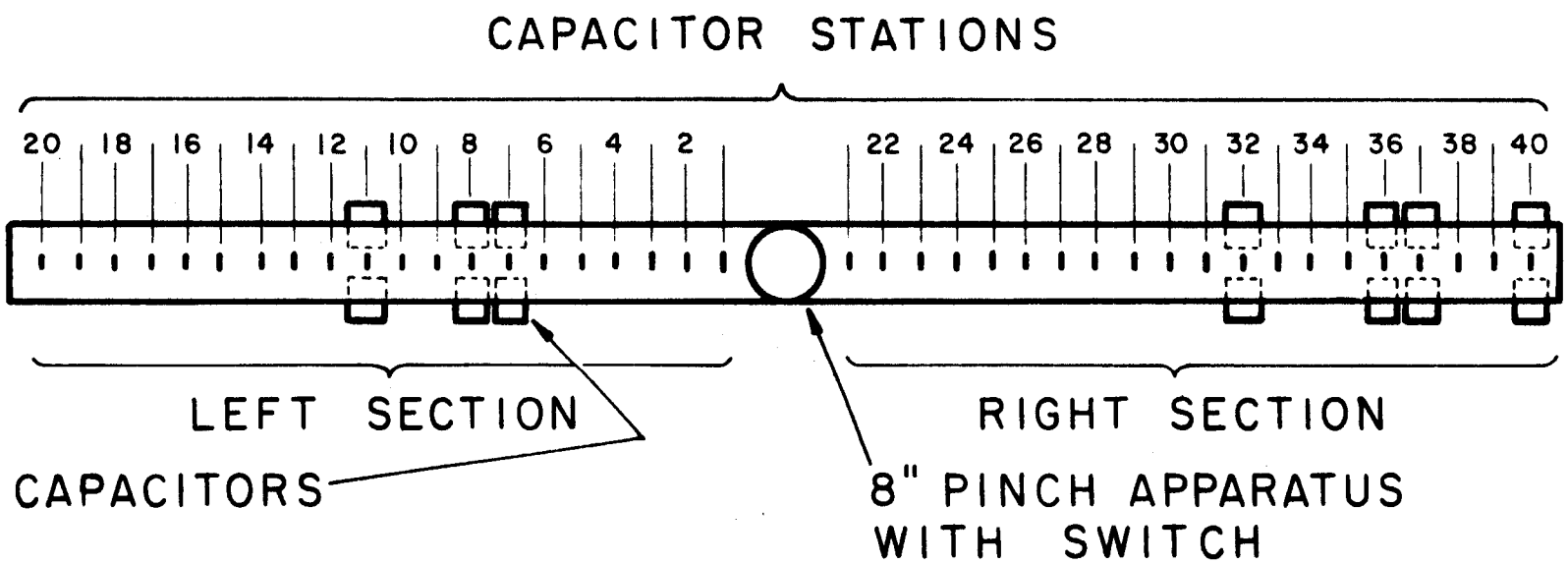

TOP VIEW OF PULSE FORMING NETWORK
(SCHEMATIC)

FIGURE 25

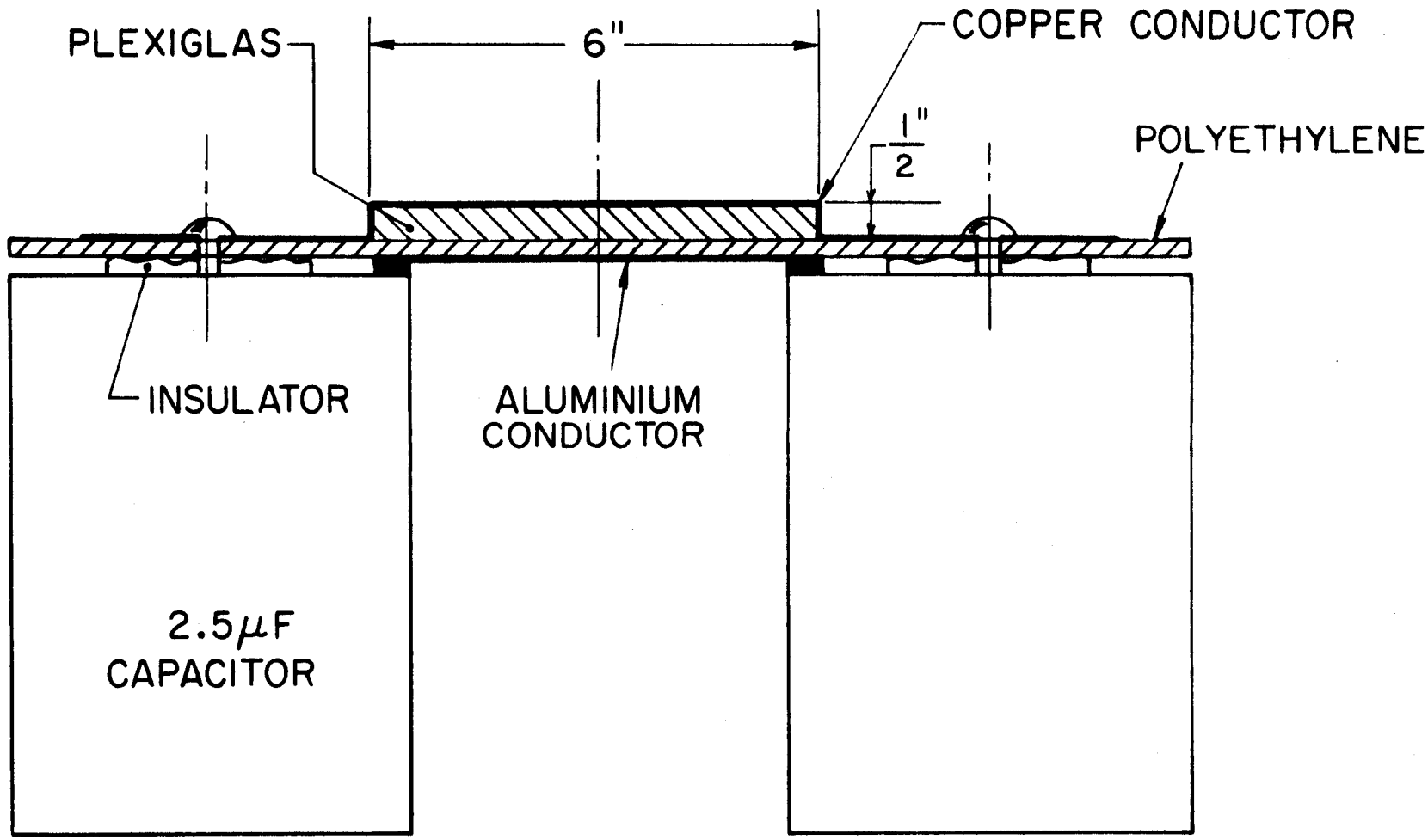

PULSE FORMING NETWORK CROSS SECTION (SCHEMATIC)

FIGURE 26

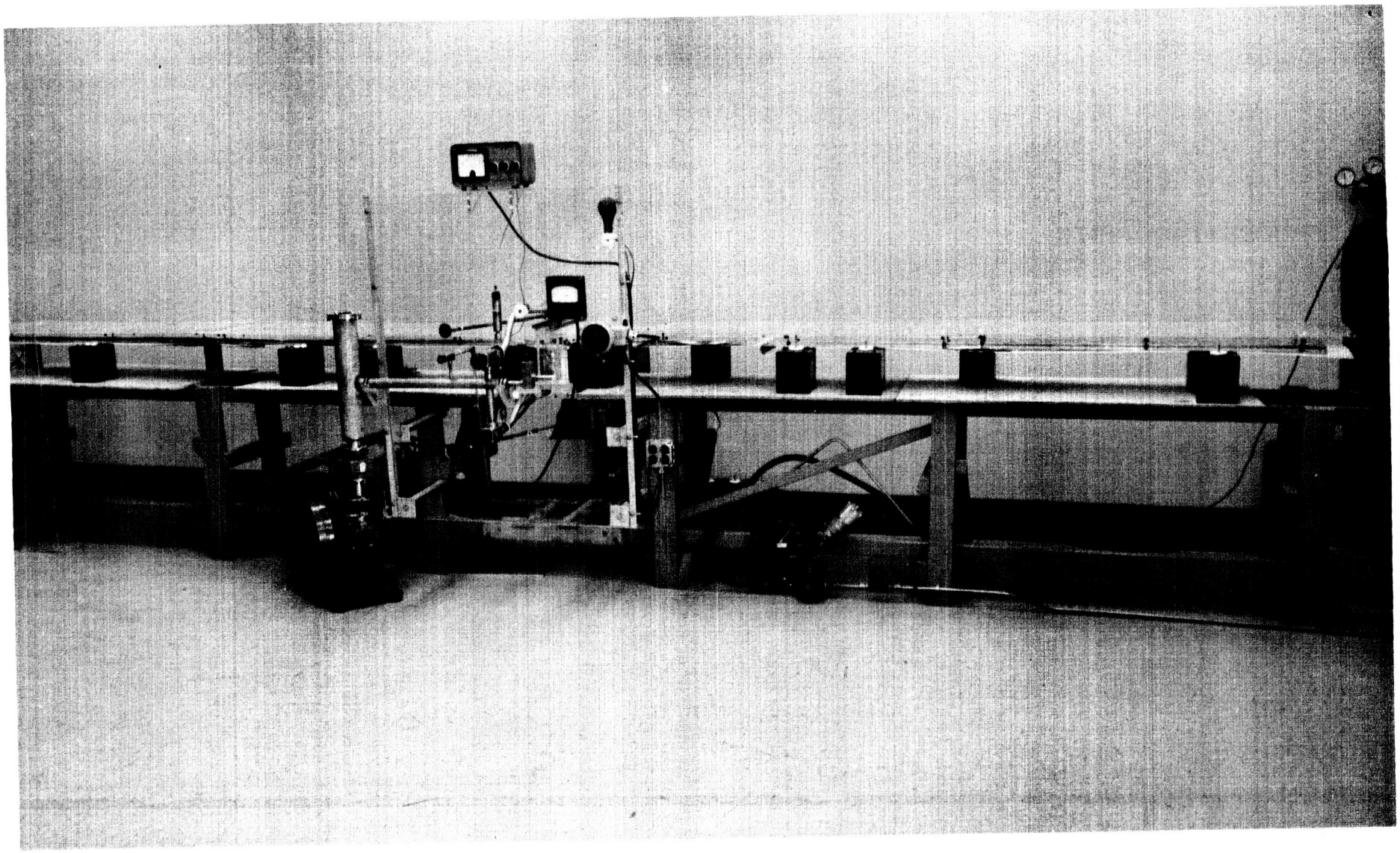

VIEW OF PULSE FORMING NETWORK

FIGURE 27

we define the following symbols and assign experimentally determined values:

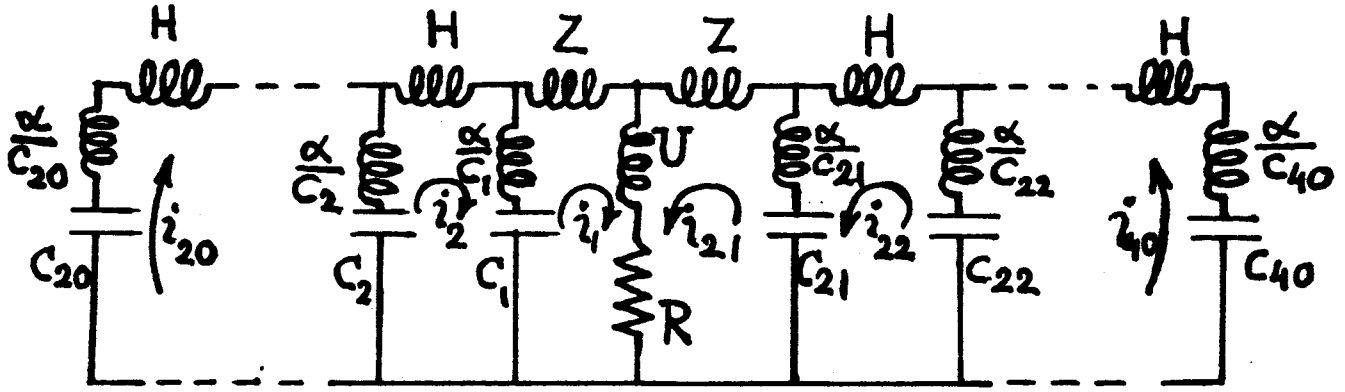

Symbol	Meaning	Value
Subscript j	Station number	1 to 40
C_j	Capacitance at station j	2.53 x 0, 1 or 2 μfd.
α	Self-inductance of capacitor and its connection to the line x capacitance	59.7 nh.-μfd.
Z	Inductance between first stations and discharge	9.2 nh.
H	Inductance between stations	17.2 nh.
R	Approximate discharge resistance	.006 ohm
U	Approximate discharge inductance	7 nh.
i_j	Current in j-th loop	(to be computed)

As in other computer studies, a very useful trick is to keep the quantities of interest of the order of unity. This can be readily accomplished by adopting a consistent set of units that fit the scale of the problem. This is not quite

the same as a nondimensional analysis of the problem, which may incidentally accomplish the same result, since equations and variables retain their dimensional nature, differing from regular units by scale changes.

We adopt as fundamental the set of quantities:

Quantity	Symbol	Value
Inductance	L_o	10 nh
Capacitance	C_o	1 μfd
Voltage	V_o	10,000 volts

Then our system of electrical units is completed by the derived quantities:

Charge	$Q_o = C_o V_o$	.01 coul.
Time	$T_o = (L_o C_o)^{\frac{1}{2}}$	0.1 μsec
Current	$I_o = Q_o / T_o$	100,000 amp.
Resistance	$Z_o = (L_o / C_o)^{\frac{1}{2}}$	0.1 ohm

The mathematical statement of the problem is then given by writing the complete set of loop voltage equations, typified by:

$$-\left(\frac{\alpha}{C_{N-1}}\right)\frac{di_{N-1}}{dt} + \left[\frac{\alpha}{C_N} + \frac{\alpha}{C_{N-1}} + H\right]\frac{di_N}{dt} - \left(\frac{\alpha}{C_N}\right)\frac{di_{N+1}}{dt} = -\frac{Q_{N-1}}{C_{N-1}} + \frac{Q_N}{C_N} \qquad (1)$$

and the relation between charge and loop currents:

$$\frac{dQ_N}{dt} = -i_N + i_{N+1} \qquad (2)$$

where Q_j is defined as the charge of the j-th station capacitance C_j. From an abstract mathematical viewpoint, we have a set of 80 first order simultaneous ordinary constant-coefficient differential equations expressible in the form

$$(A)(\dot{X}) = (B)(X) \qquad (3)$$

Where (A) and (B) are 80x80 coefficient matrices, and (X) and $(\dot{X})$ 80 element column vectors of the unknowns and their time-derivatives. Prior to any numerical integration scheme we must deal with the linear algebra problem of obtaining

$$\dot{X} = (A)^{-1} (B) (X) \tag{4}$$

so that the time derivative of each dependent variable is expressed in a fashion that involves no other time derivatives. The formidable inversion of an 80x80 matrix fortunately can be circumvented by noting that the 40 charge equations typified by (2) are already in the desired form for integration. Also, in the loop-voltage equations, only loops 1 and 21 have currents in their right-hand side terms. We then attack the simpler problem

$$\begin{pmatrix} A \\ (40x40) \end{pmatrix} \begin{pmatrix} \frac{di_1}{dt} \\ \vdots \\ (40x1) \\ \vdots \\ \frac{di_{40}}{dt} \end{pmatrix} = \begin{pmatrix} B \\ (40x42) \end{pmatrix} \begin{pmatrix} Q_1 \\ \vdots \\ (42x1) \\ \vdots \\ Q_{40} \\ i_1 \\ i_{21} \end{pmatrix} \tag{5}$$

requiring the less-demanding inversion of the 40x40 matrix A.

The initial conditions are quite simple:

$$\begin{aligned} i_j(0) &= 0 \qquad\qquad j = 1 \text{ to } 40 \\ Q_j(0) &= V(0)C_j = C_j \end{aligned} \tag{6}$$

since we always take V(0) = 10,000 volts which is unity in the characteristic units of the problem.

With the problem thus defined, a FORTRAN program was prepared for the University's IBM 7094 machine. The larger program was broken into several "subroutines" which are small enough that the

logic is easy to follow and can be individually corrected without affecting the rest of the program. As programmed, about 80% of the 7094 core storage was required.

For programming simplicity every configuration is treated as a 40 loop problem. To avoid singularities in the computations arising from zero values of capacitance, the program places .001 μfd at any station for which the input data specifies zero capacitance. The price of this programming simplification is increased average time to compute each case; all configurations require approximately the same time as the most complex. In operation, a single punched card bearing an identifying case number and 40 integers, which are all 0, 1, or 2, is the complete input for one case.

The program returns numerical values and a graph "drawn" by the off-line high speed printer. Figure 28 shows one such graph. While the computations are performed in the characteristic units we have defined, the results are presented in conventional units. Loop currents 1 and 21 are the net contributions to the discharge current of the left and right wings respectively of the pulse-forming network. They would be independent of each other in the limit of zero load impedance. Their sum is the discharge current. At the bottom of the graph the configuration of the capacitors is displayed showing the number of units at each station. Integration is terminated when the load current becomes negative. The 7094 computes a single case, including preparation of the graph, in about 50 seconds.

Selected results of computations of this type indicate that a broad spectrum of current pulse shapes is indeed available with this device. Pulses of rising and falling characteristics, rectangular pulses of various amplitudes and length, and various amplitude and frequency sine waves have been demonstrated, as well as many more pathological waveforms. This catalogue will prove highly useful as we acquire more experience with the dependence of the dynamical processes in the discharge on the applied pulse shape.

Our first experimental studies with the pulse-forming discharge device have been largely confined to two diverse current shapes: a damped sine wave, and a quasi-rectangular pulse with a slowly rising top, of amplitude comparable to the sine wave. Figure 29 is a comparison of typical streak photographs and the corresponding current waveforms obtained in 120 μ Argon. The sine-driven discharge shows the characteristic patterns of multiple luminous fronts and a velocity which decreases towards the center. The pulse-driven discharge shows only one luminous front which accelerates throughout its inward excursion, reaching a terminal velocity 4 or 5 times as great as the sine-driven case.

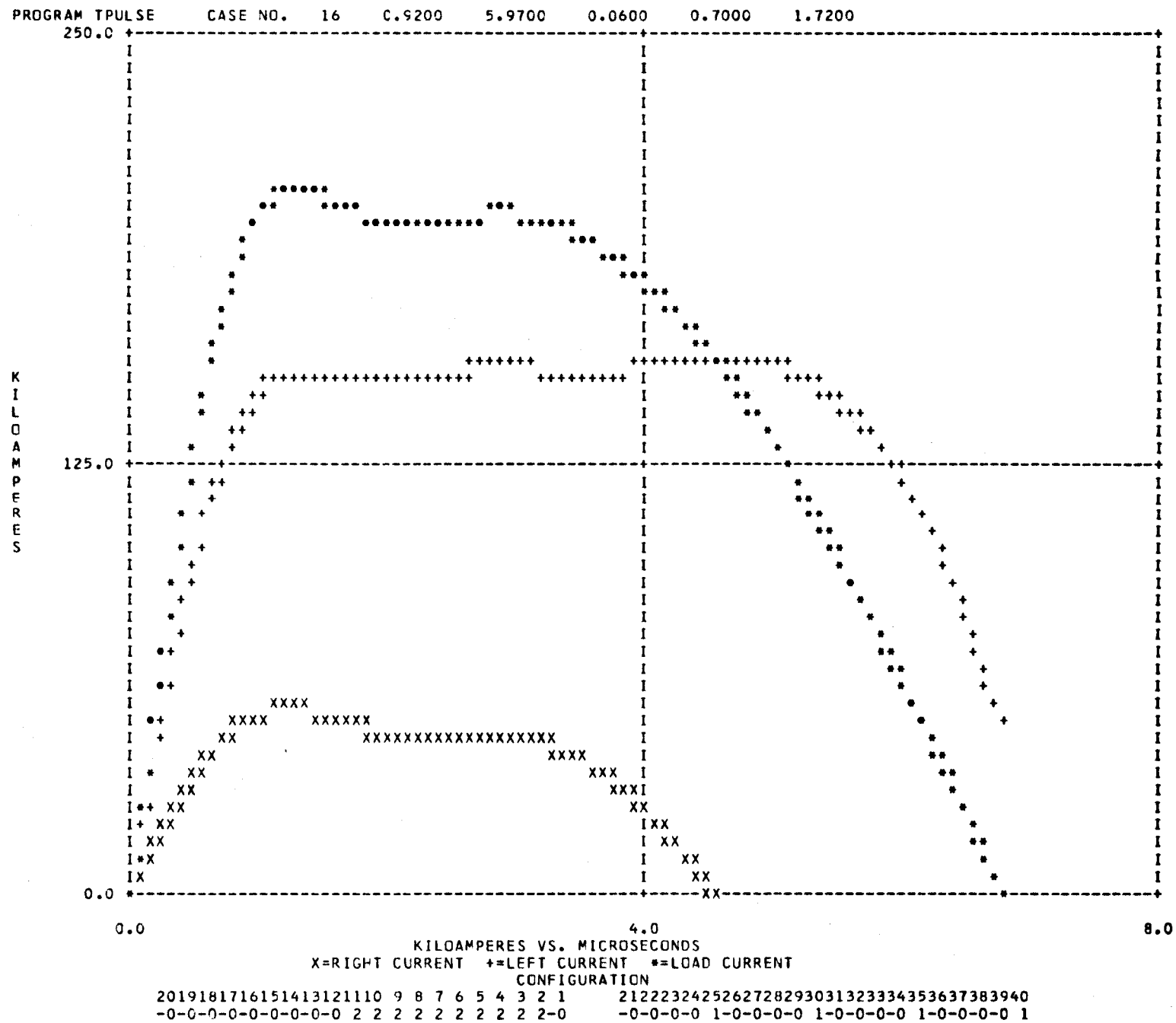

FIGURE 28

TYPICAL PULSE NETWORK PROGRAM OUTPUT

AP25-P14-65

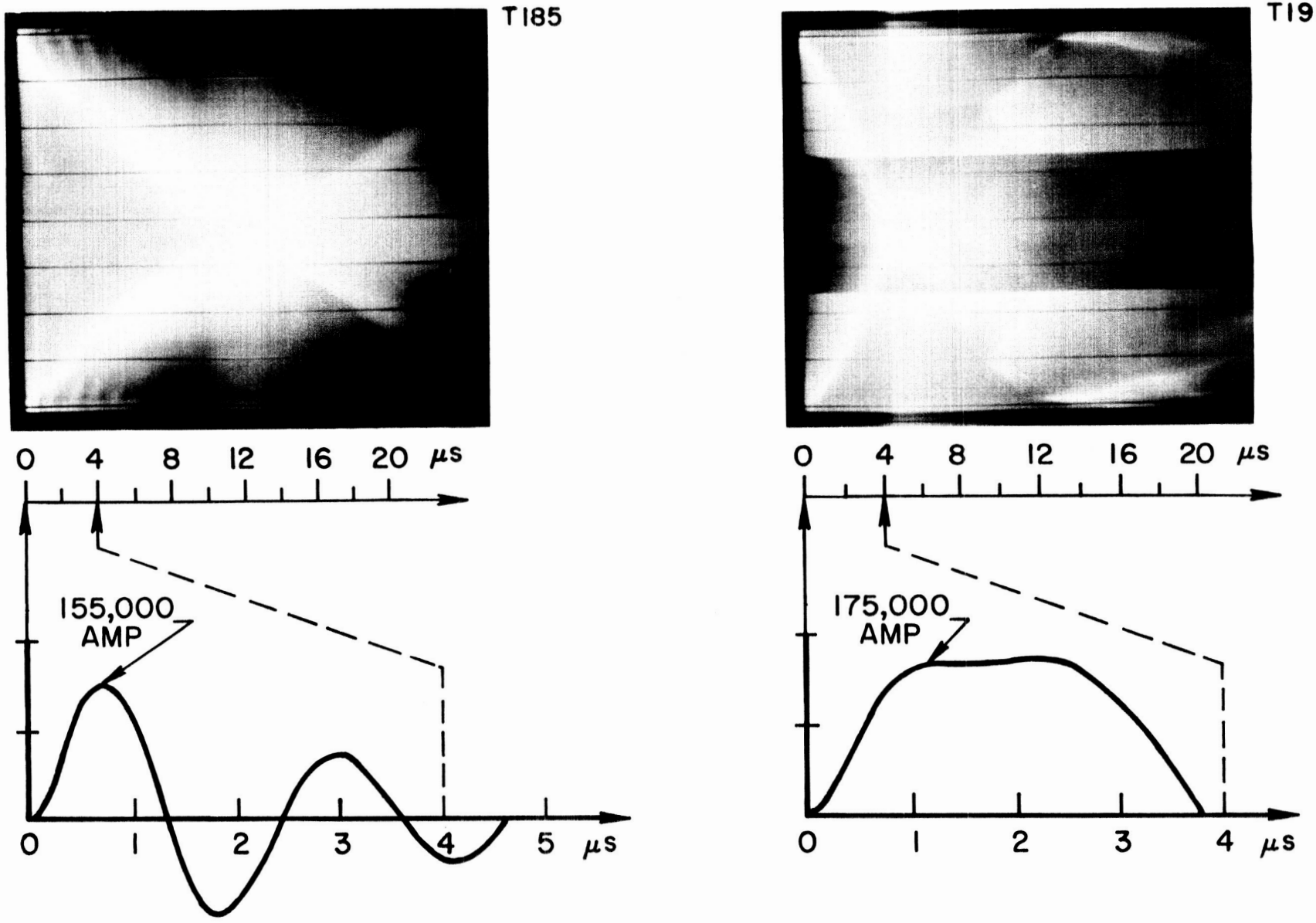

8" PINCH DISCHARGE IN 120 μ ARGON
FOR TWO CURRENT WAVEFORMS

FIGURE 29

The appearance of only one luminous front presumably implies that only one current sheet is formed, which thus will be coupled to the external circuit throughout its entire radial motion. The extreme improvement that is in fact realized in this regard is illustrated in Fig. 30 which compares unintegrated magnetic probe records for the two types of discharge. In these records, the probe response is essentially indicative of the local current density at the probe position. The rectangular pulse-driven current sheets are seen to be of substantially greater amplitude and to propagate further than the corresponding sine-wave results. The extent to which this performance can further be improved by invoking other than rectangular pulse shapes is currently under study.

A more complete report on the experimental and theoretical results of this program will be presented at the San Francisco Meeting of the AIAA in July, 1965. In addition, this work will be discussed in full in the Ph.D. thesis of Mr. Neville A. Black, to be submitted this Spring.

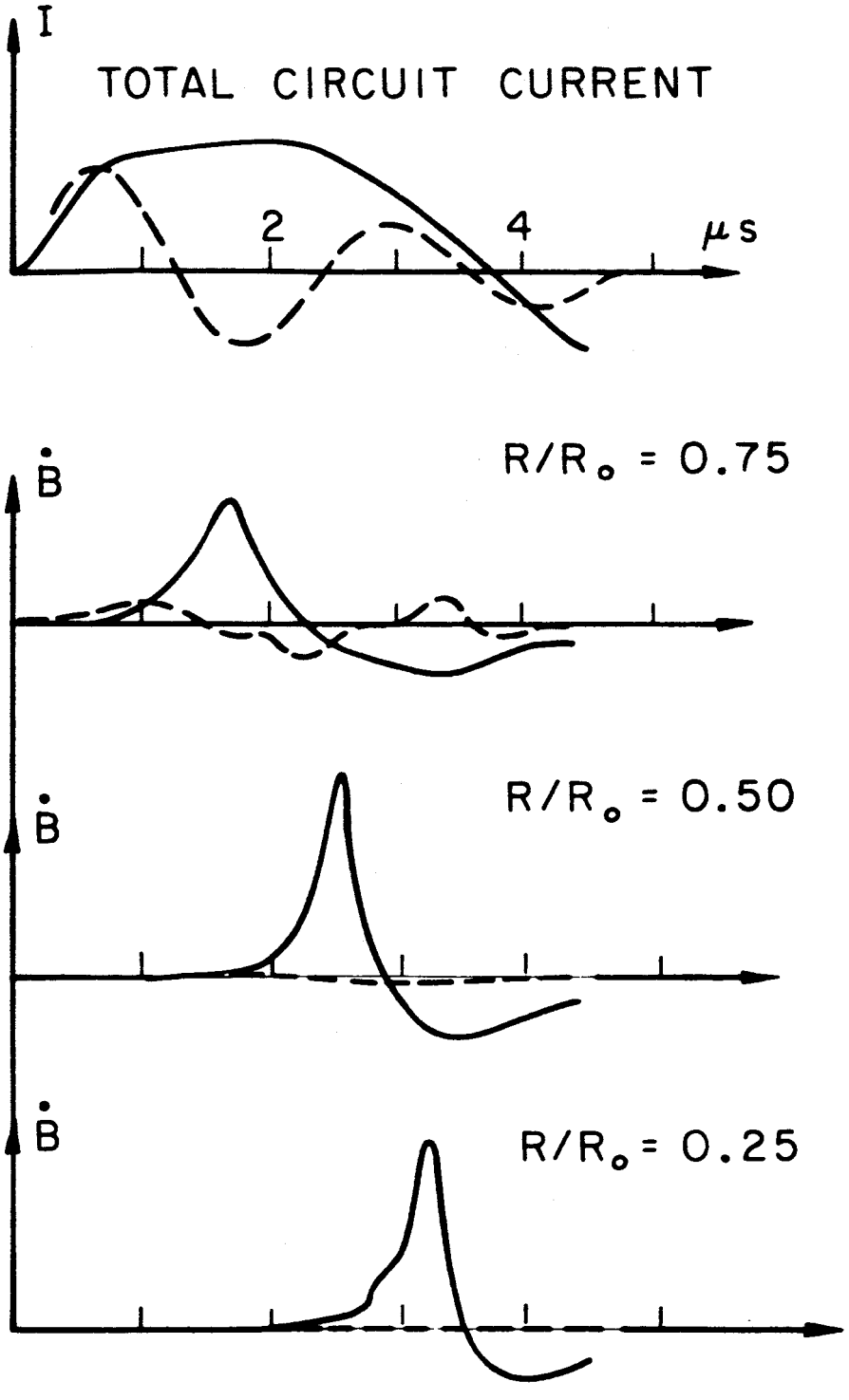

COMPARISON OF MAGNETIC PROBE RESPONSES
FOR TWO CURRENT WAVEFORMS

FIGURE 30

IV. MICROWAVE STUDIES
(Ellis)

The motivation for initiating a microwave probe study of the discharge has been discussed in the previous semi-annual report (13), where some preliminary results were presented. These results have now been extended considerably to three different working gases--Argon, Helium, and Nitrogen--over a range of pressures from 30 μ to 1 mm, and over a time scale covering six orders of magnitude, 10^{-8} - 10^{-2} sec.

The probe itself consists of a 70 g.c. (λ = 4 mm) signal source, a waveguide and associated circuitry for transmitting the microwaves, and a specially designed horn antenna matched to free space, for the purpose of admitting microwave radiation into the discharge region. As shown in Fig. 31, and the sketch below, entrance is made through an upper electrode designed specifically for this purpose, with appropriately spaced apertures for varying the radial position of the probing antenna.

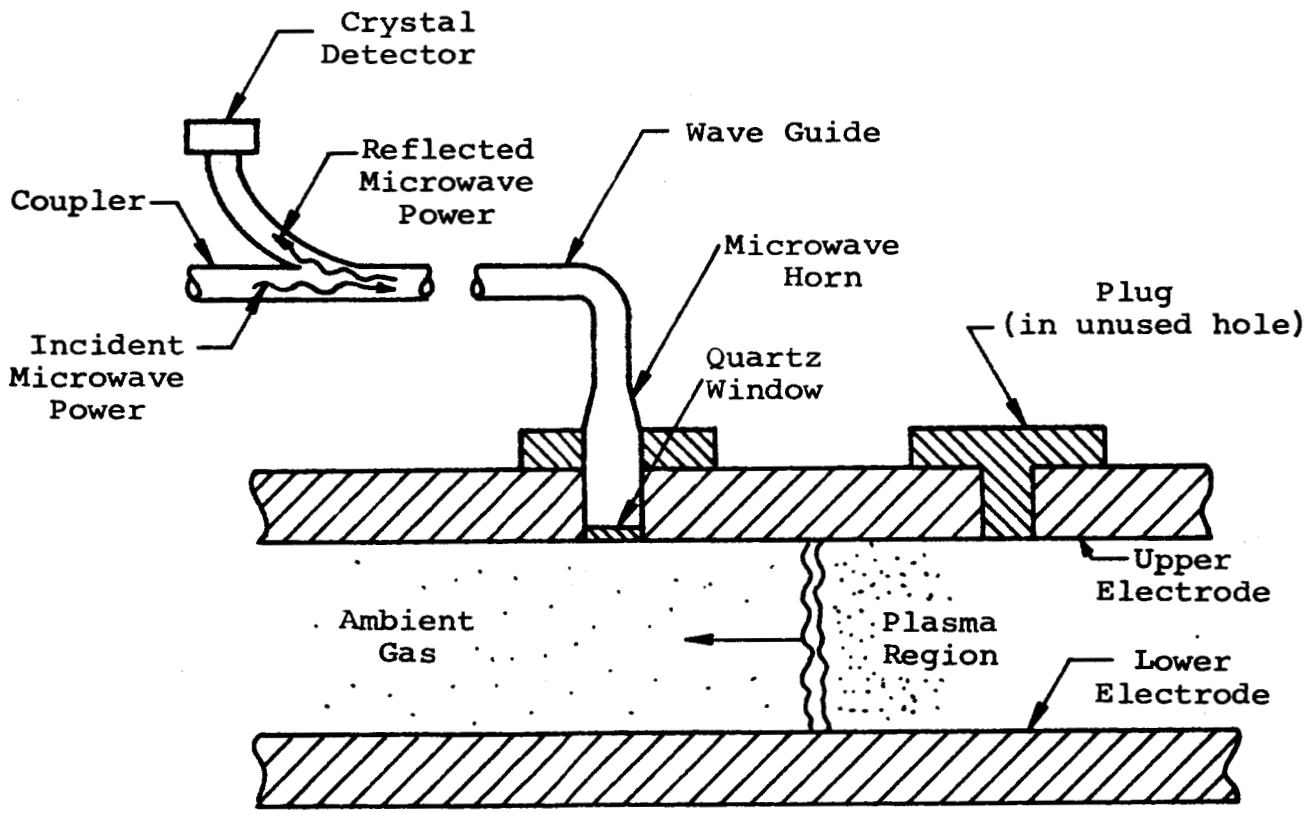

The microwave power reflected from the ionized gas near the horn aperture is recorded as a function of time on a dual beam oscilloscope simultaneously with a Rogowski coil current signal used for calibration purposes.

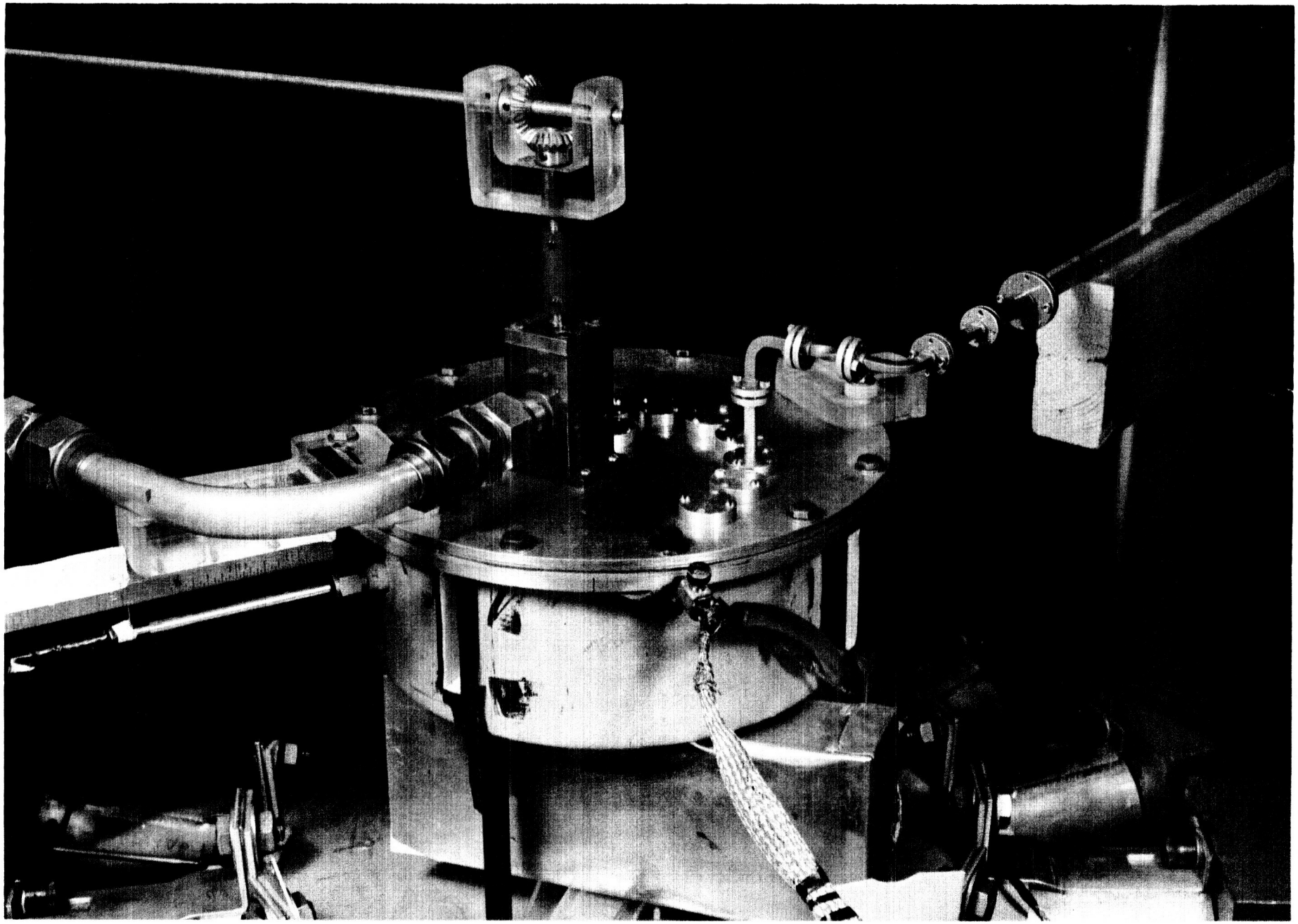

8" PLASMA PINCH CHAMBER WITH ELECTRODE
FOR μ-WAVE PROBING

FIGURE 31

Figures 32 and 33 show two typical oscillograms on widely different time-base, which illustrate the essential features of a typical reflected power signal. Also indicated on these figures are seven characteristic times, Δt_1 - Δt_7, which are useful in correlating the data in terms of the development of three significant phases of the reflected power signal: the initial rise, a characteristic dip late in the discharge, and the final decline.

Δt_1: Time at which reflected signal is first observed. This is a characteristic delay time between the start of the current and the appearance of a minimum detectable level of free electrons ($\sim 10^{12} cm^{-3}$) in the discharge. In Argon, for example, this delay is typically about 0.4 μsec at which time a signal is detectable almost simultaneously over the entire chamber (see Fig. 34). In Helium, Δt_1 is about 0.2 μsec; in Nitrogen, about 0.4 μsec.

The lowest pressure discharges (30 μ) are somewhat anomalous in this respect, showing smaller Δt_1's for all three gases at nearly all positions. This supports other evidence (e.g. Kerr cell photographs) that the nature of the discharge is substantially different at very low pressures.

This first response of the probe can be ascribed either to the presence of an ionizing precursor front, far ahead of the main current pulse, or to some phenomenon in the breakdown process, such as a glow discharge over the entire electrode area. This latter interpretation avoids the concession of near-infinite precursor velocities.

Δt_2: Time at which reflected signal first reaches half-maximum. Since this time can be located more precisely than Δt_1, it is possible to assign, in terms of Δt_2, a well-defined, finite propagation velocity to the precursor in the higher pressure discharges (Fig. 35). This velocity ranges up to several percent of the velocity of light in some cases. Fig. 36 shows the pressure dependence of this delay time in argon, at various radial positions. This pressure dependence is seen to be weak above 100 μ. The minimum delay occurs at radial position $\frac{R}{R_o} = \frac{7}{8}$ for all pressures, indicating the discharge originates in this region rather than exactly at the insulator wall itself. This result supports the magnetic probe data which also shows the current sheet to form a short distance inward from the insulator wall.

Δt_3: Time from first appearance of signal to half reflection. This time is a measure of the rate at which the electron density

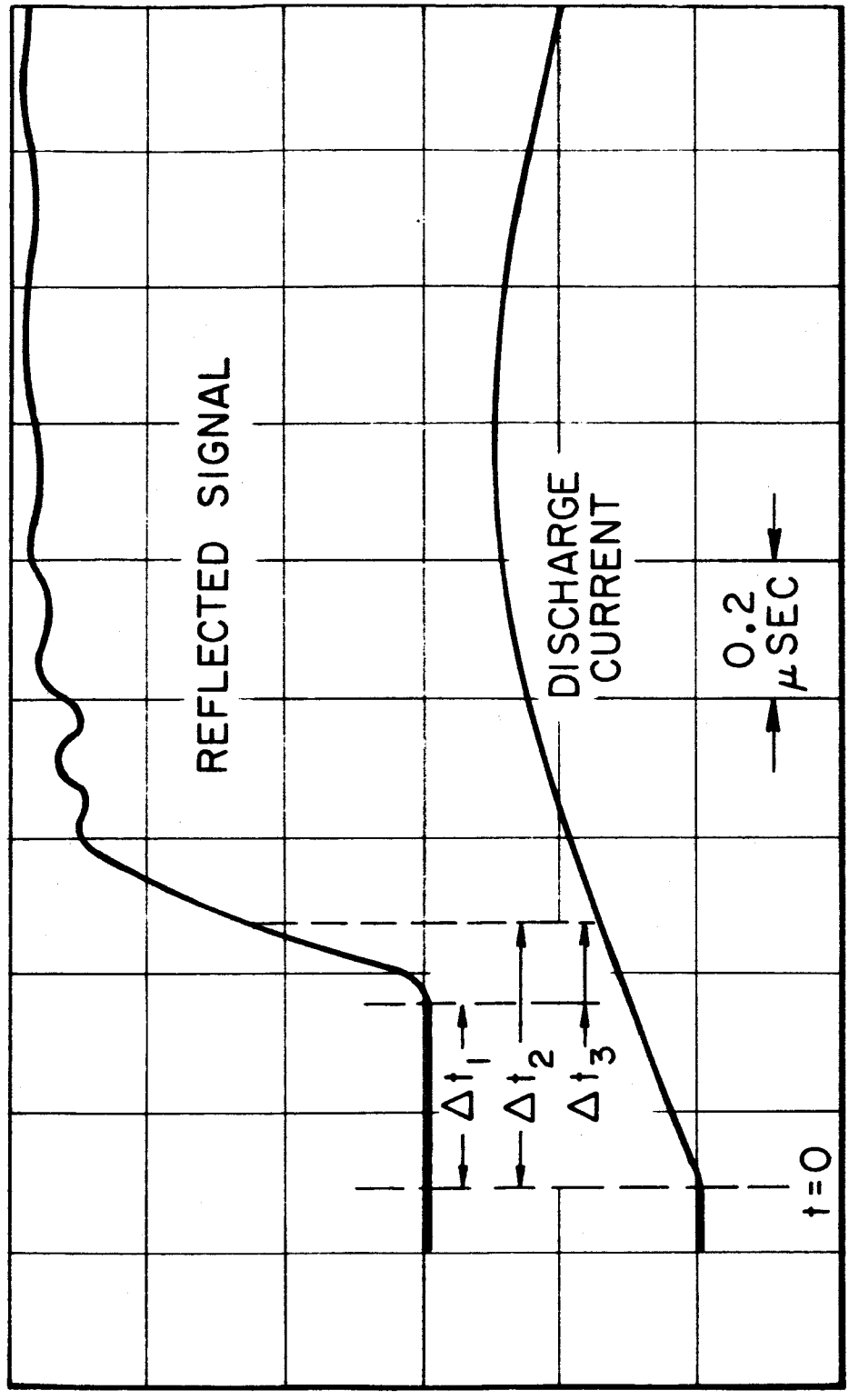

70 GC REFLECTION AT $R/R_0 = .75$
120 μ ARGON

FIGURE 32

JPR 2300A

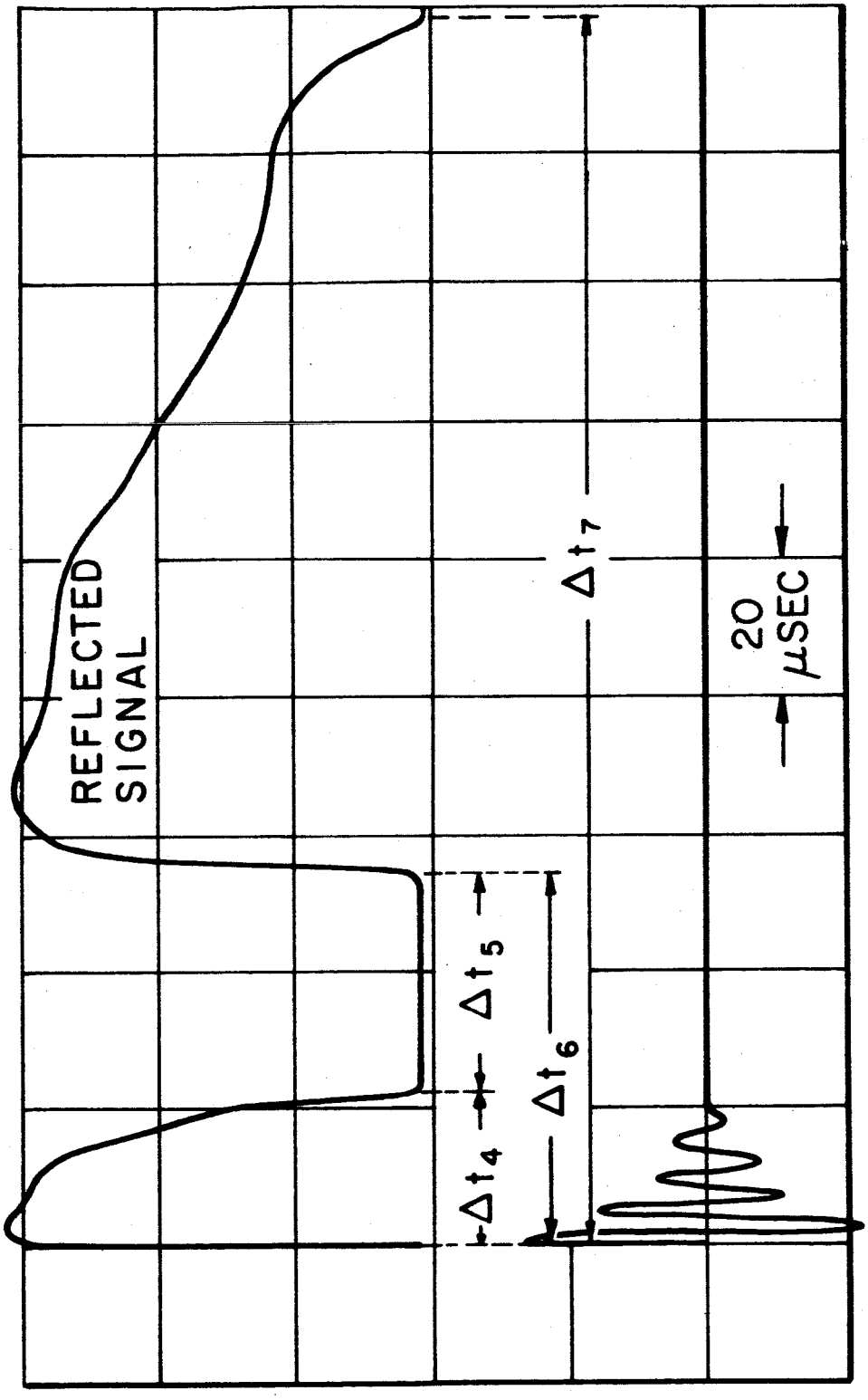

70 GC REFLECTION AT CENTER OF CHAMBER
120 μ ARGON

FIGURE 33

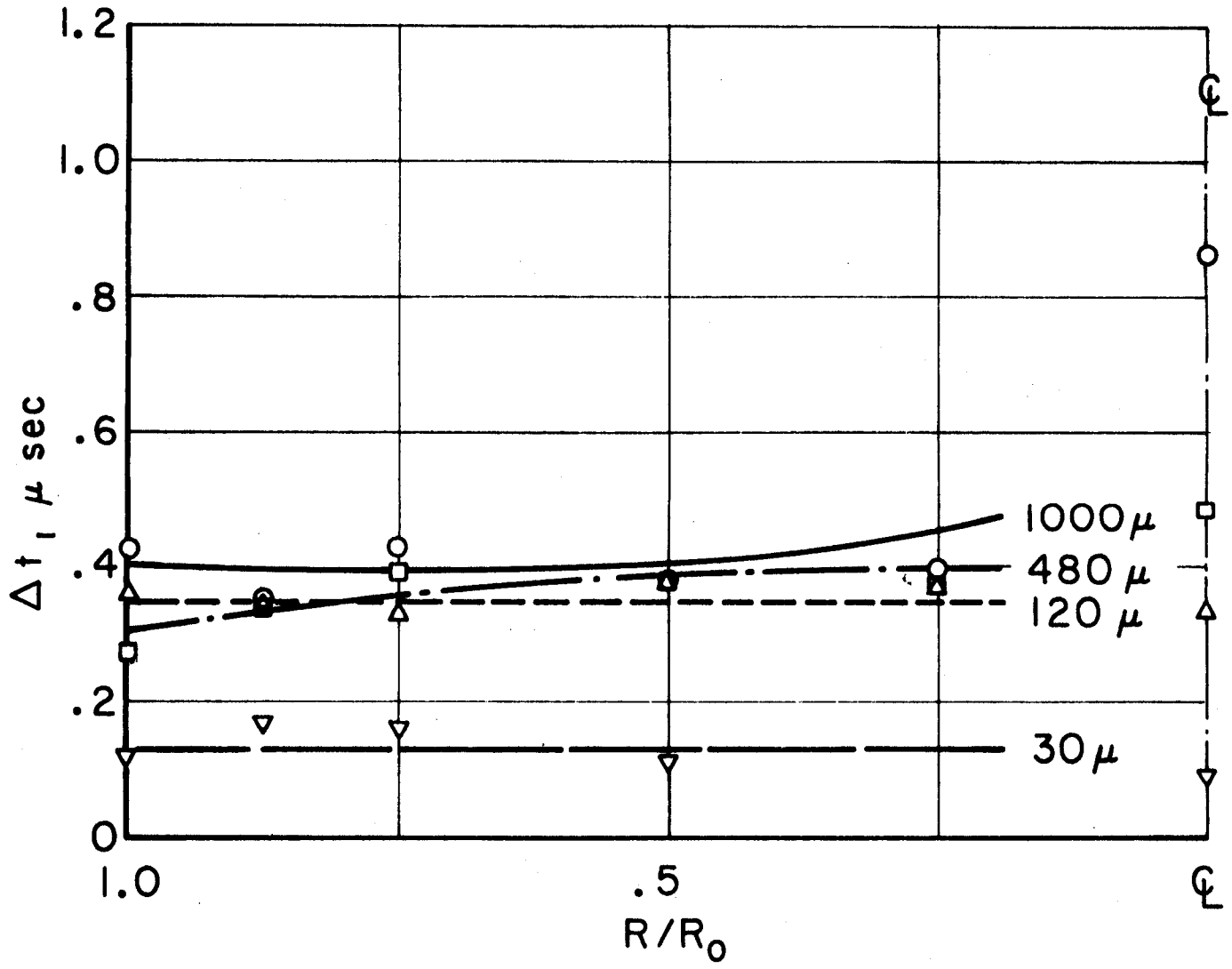

8" PINCH DISCHARGE IN ARGON: ELAPSED TIME TO INITIAL INTERCEPT VS RADIAL POSITION, 70 GC

FIGURE 34

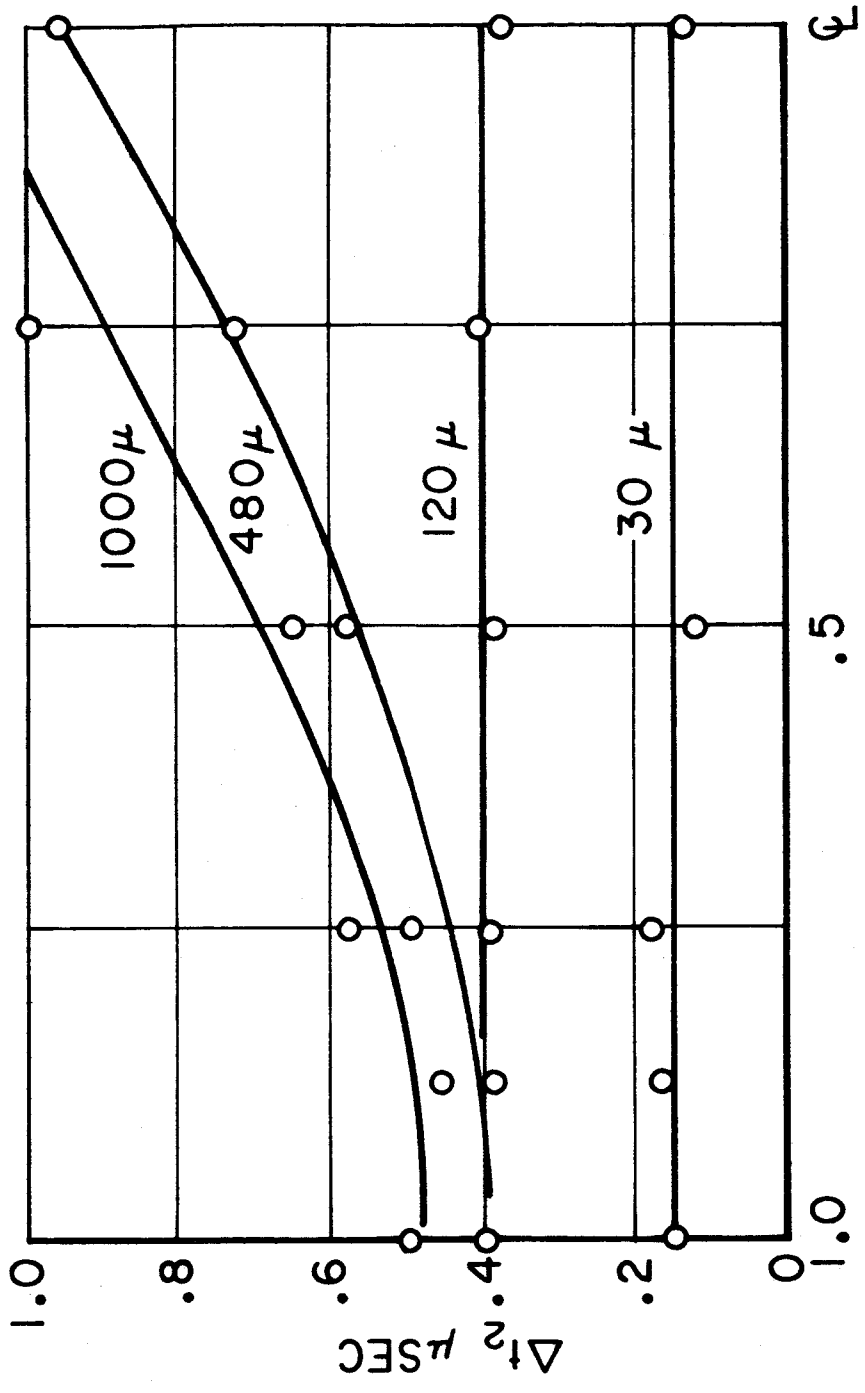

8" PINCH DISCHARGE IN ARGON:
TIME TO 1/2 MAX REFLECTION OF 70 GC

FIGURE 35

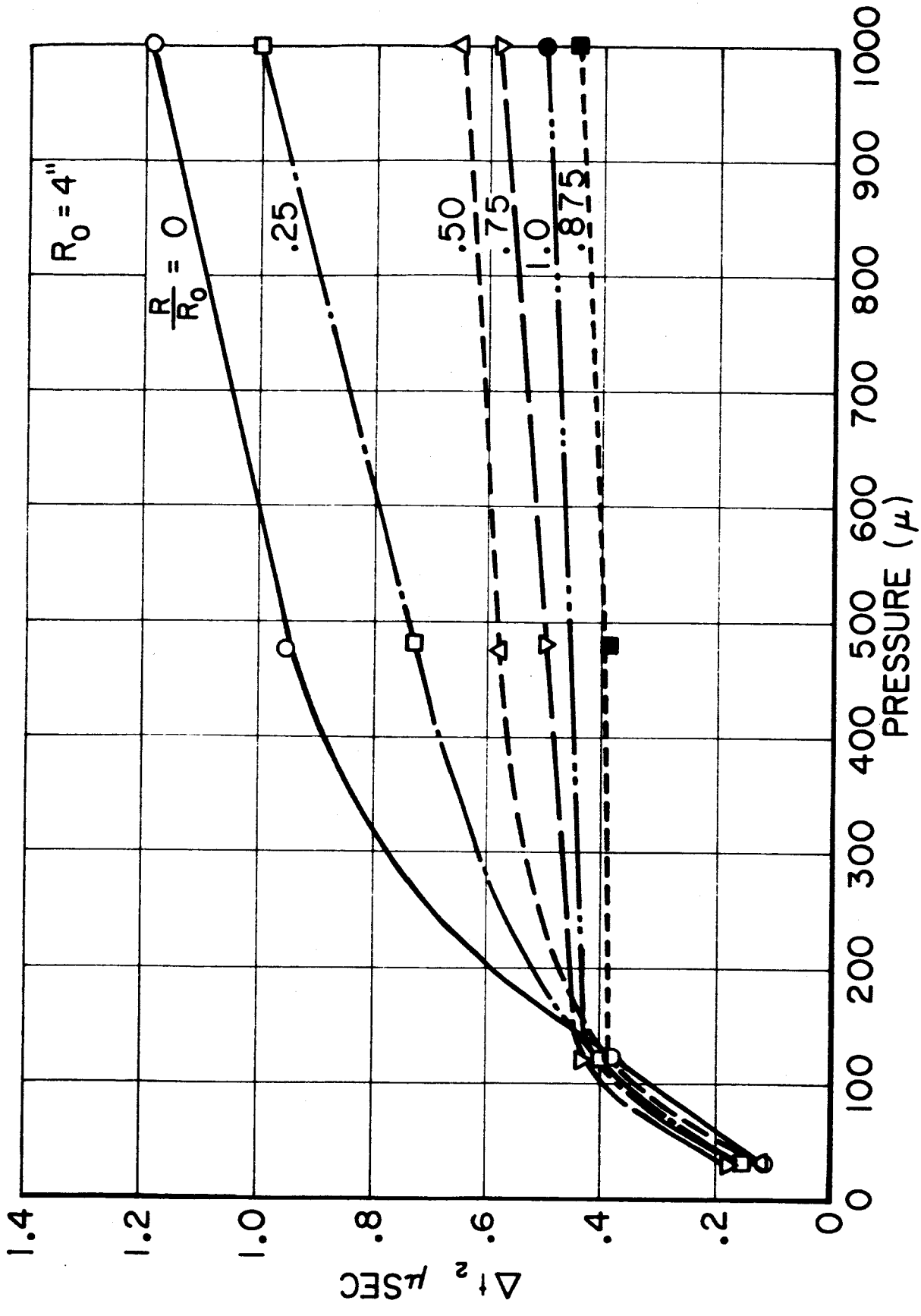

FIGURE 36

rises from a detectable minimum to the critical density, i.e. $10^{12} - 10^{14} cm^{-3}$. Δt_3 probably embraces two phenomena: 1) the finite time for ionization collisions to increase the electron density to these levels, and 2) the finite time required for the ionizing front to move across the horn aperture.

A general conclusion to be drawn from Δt_3 data is that, for all three gases the rate of electron density growth during the precursor phase, is largest near the wall and diminishes as the precursor approaches the center (see Fig. 37).

Δt_4: Time of appearance of a very pronounced dip (Fig. 33) in the reflected signal. This dip occurs in all gases investigated at times long compared to the discharge ringdown. The dip is always more prominent at the center of the machine, rapidly diminishing in strength as the probe is moved outward. The most pronounced effect occurs in nitrogen, where the dip is positively identified at radii of $R/R_o = \frac{1}{2}, \frac{1}{4}, 0$. In helium it is observed at $R/R_o = \frac{1}{4}, 0$ and in argon only at the center of the pinch. For all pressures above 100 μ, the ordering $\Delta t_{4_{He}} < \Delta t_{4_{N_2}} < \Delta t_{Ar}$ is observed.

The dip occurs earliest at the low pressures and, in general, simultaneously at all positions where it can be observed. In all three gases the leading edge of the dip is less well-defined than the trailing edge, i.e., it begins rather smoothly and ends very abruptly.

Δt_5: Time duration of the dip. The duration of this period of low electron density is essentially independent of the type of gas, pressure, and probe position. Typically it is about 15-20 μsec.

Δt_6: Time of the sudden rise in reflected signal which ends the dip. Since the discharge has already dissipated itself quite thoroughly by the time this event occurs, the sudden increase in electron density here can only be attributed to a gasdynamic event rather than to further discharge activity. In fact, the entire appearance of the dip, beginning as it does quite gently, long after pinch time, and terminating so abruptly, is suggestive of the passage of a rarefaction wave past the probe, followed sometime later by a strong compression or shock.

For example, the reflection of the pinch at the center line of the chamber will produce a classical peaked shock profile propagating outward. That is, the reflected shock will be followed by a rarefaction phase which cools and expands the gas. At some

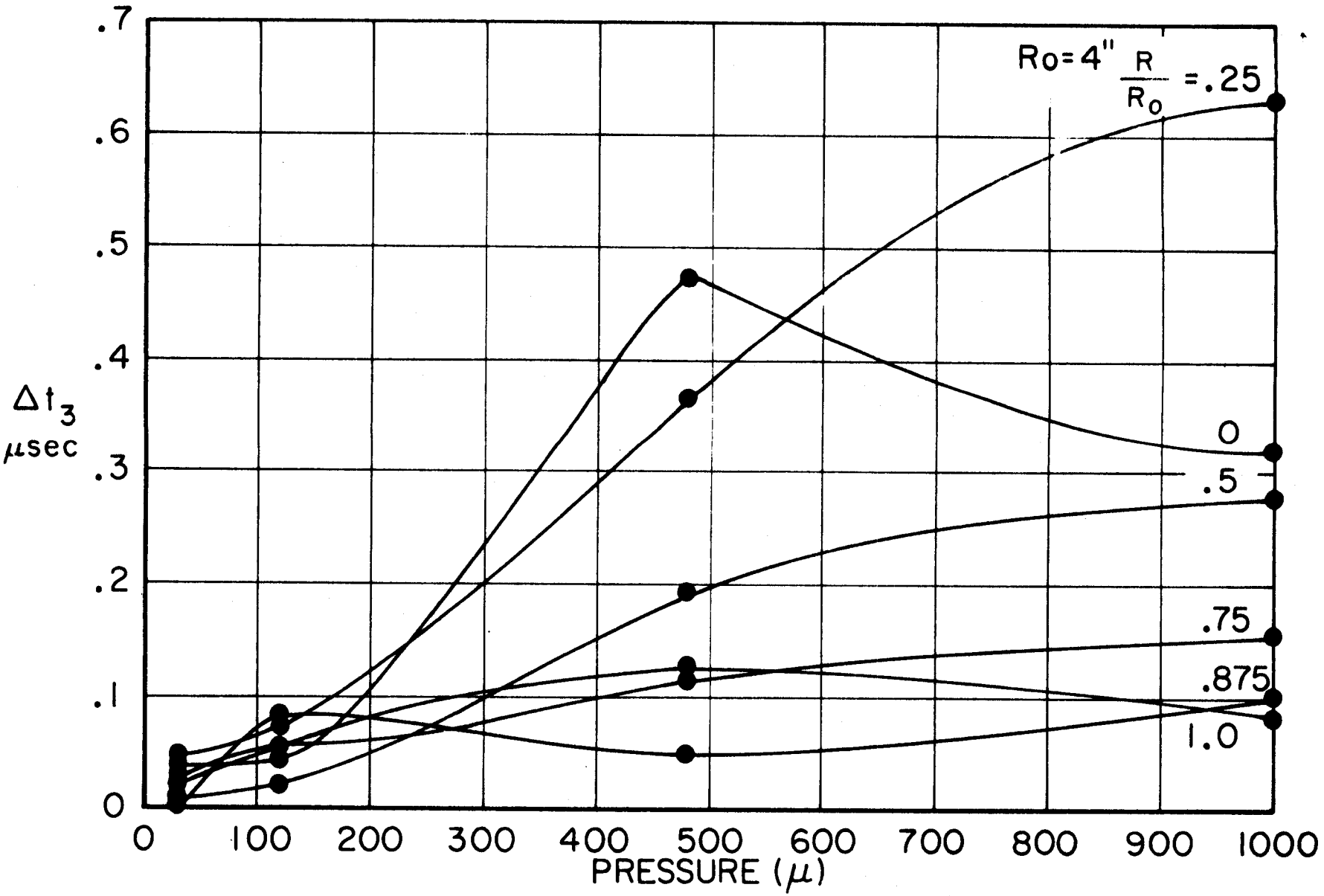

8" PINCH DISCHARGE IN NITROGEN:
Δt_3, TIME FROM INITIAL INTERCEPT TO 1/2 MAX. REFLECTION
vs PRESSURE, 70 GC

FIGURE 37

point in the wake of this reflected shock, therefore, the electron density may reduce below cutoff, where it will remain until the shock front re-reflects from the outer wall and returns past the observation station.

To check this hypothesis, the extents of the dips have been superimposed on corresponding streak photographs for the three gases Argon, Helium, and Nitrogen. The results are sketched in Figs. 38-40. Note that the end of the microwave dip at the center position exactly coincides with the arrival of the reflected luminous front as shown in the streak photographs. Furthermore, the dip begins appreciably after the first reflection of the luminous fronts from the center, indicating that the electron density in the pinch column may be several orders of magnitude above the critical value for 4 mm microwaves ($10^{14}cm^{-3}$) requiring an extensive rarefaction period before any dip is apparent. The observed ordering of dip time of arrival, Δt_4, for the three gases corresponds to the time scale of the luminous events for the same gases.

Δt_7: Time for final decline of the reflected signal. This must represent the time necessary for recombination and other losses to reduce the electron population below the detectable level. In Argon (Fig. 41) we see evidence of rapid quenching in the regions of the cold outer wall, and in the hot, high pressure pinch column in the center. The higher ionization levels persist mainly as a toroidal region at about 1/2 chamber radius.

Both argon and helium show ionization persistence increasing in a smooth way with increasing pressure at all positions (Fig. 42). But nitrogen shows markedly different behavior at high pressures, where ionization times become quite short. This may be due, in part, to the radically different recombination processes available in a diatomic gas.

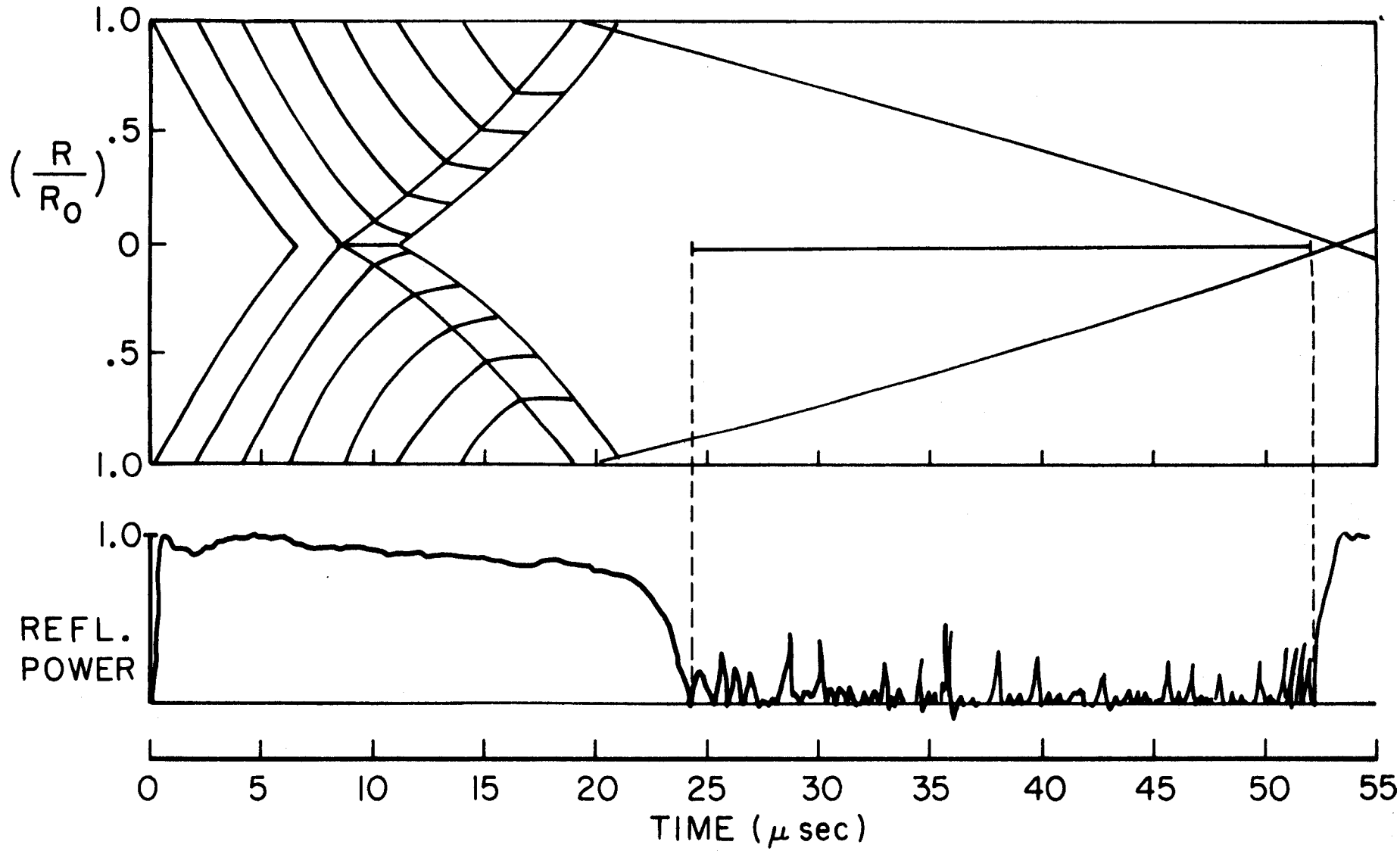

FIGURE 38 REFLECTION COEFFICIENT & STREAK PICTURE IN 8" ARGON AT 120 μ

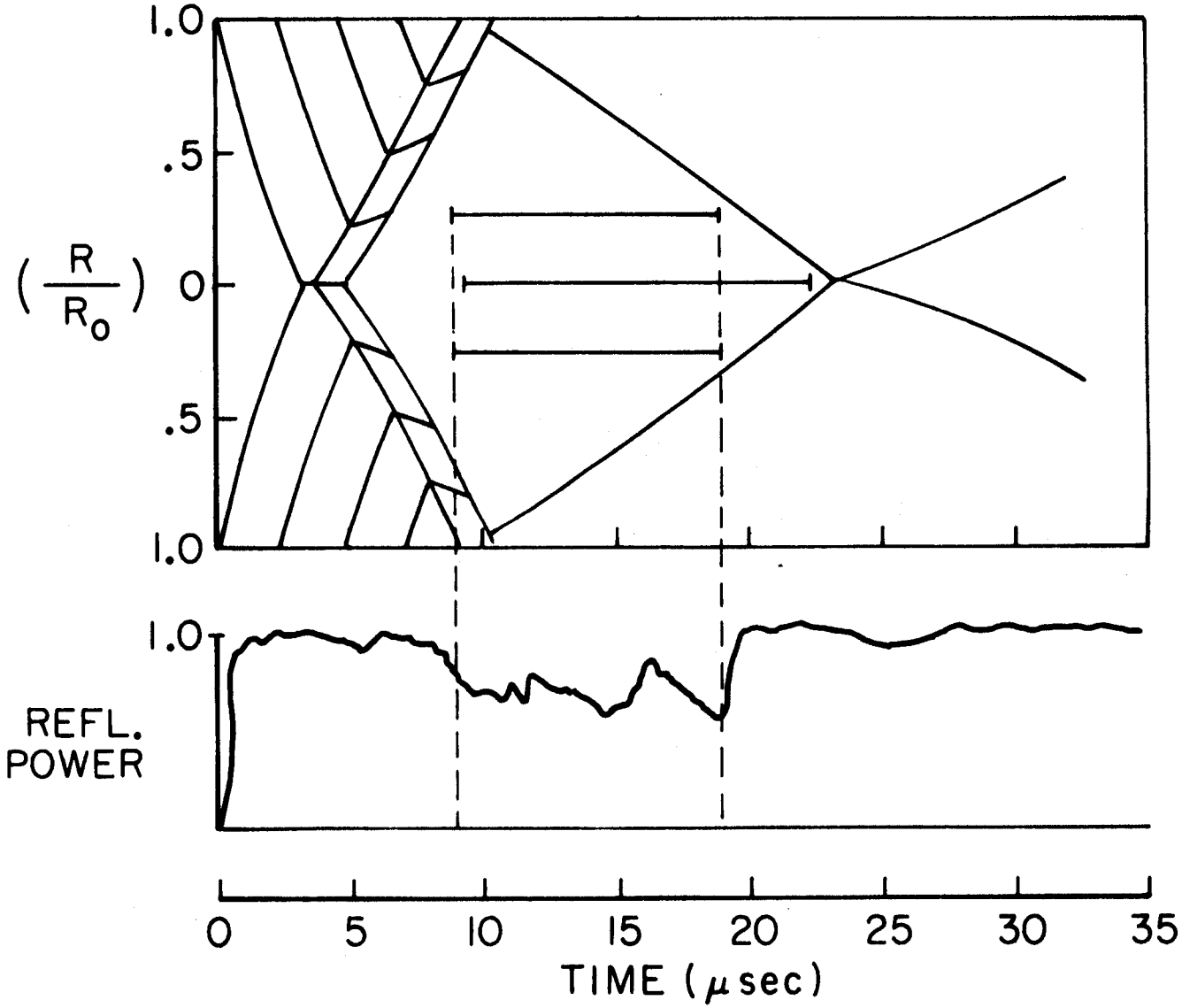

REFLECTION COEFFICIENT & STREAK PICTURE IN 8" HELIUM AT 300 μ

FIGURE 39

AP25-JFK-2044-65

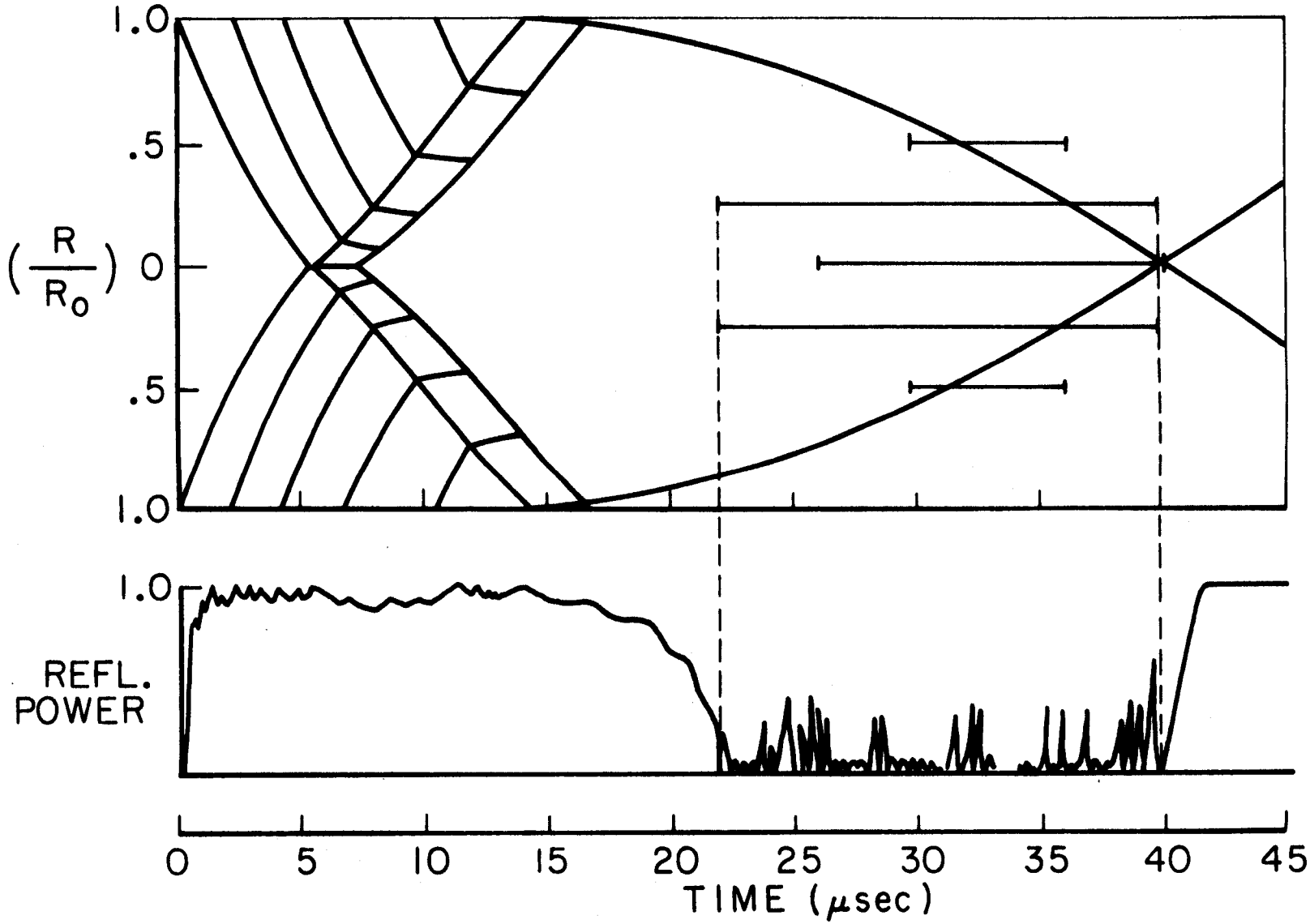

FIGURE 40 REFLECTION COEFFICIENT & STREAK PICTURE IN 8" NITROGEN AT 100μ

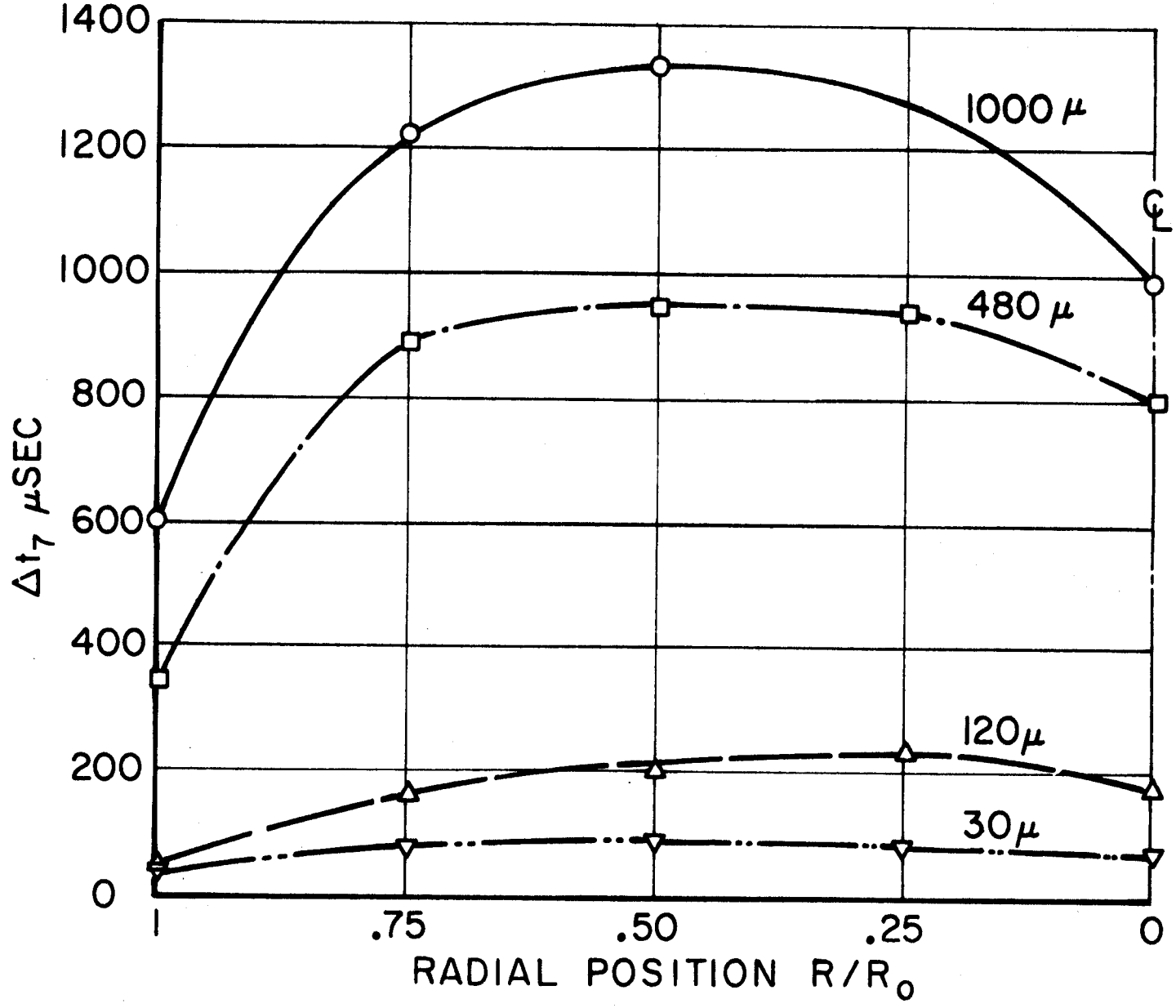

8" PINCH DISCHARGE IN ARGON:
Δt_7, IONIZATION TIME vs RADIAL POSITION, 70 GC

FIGURE 41

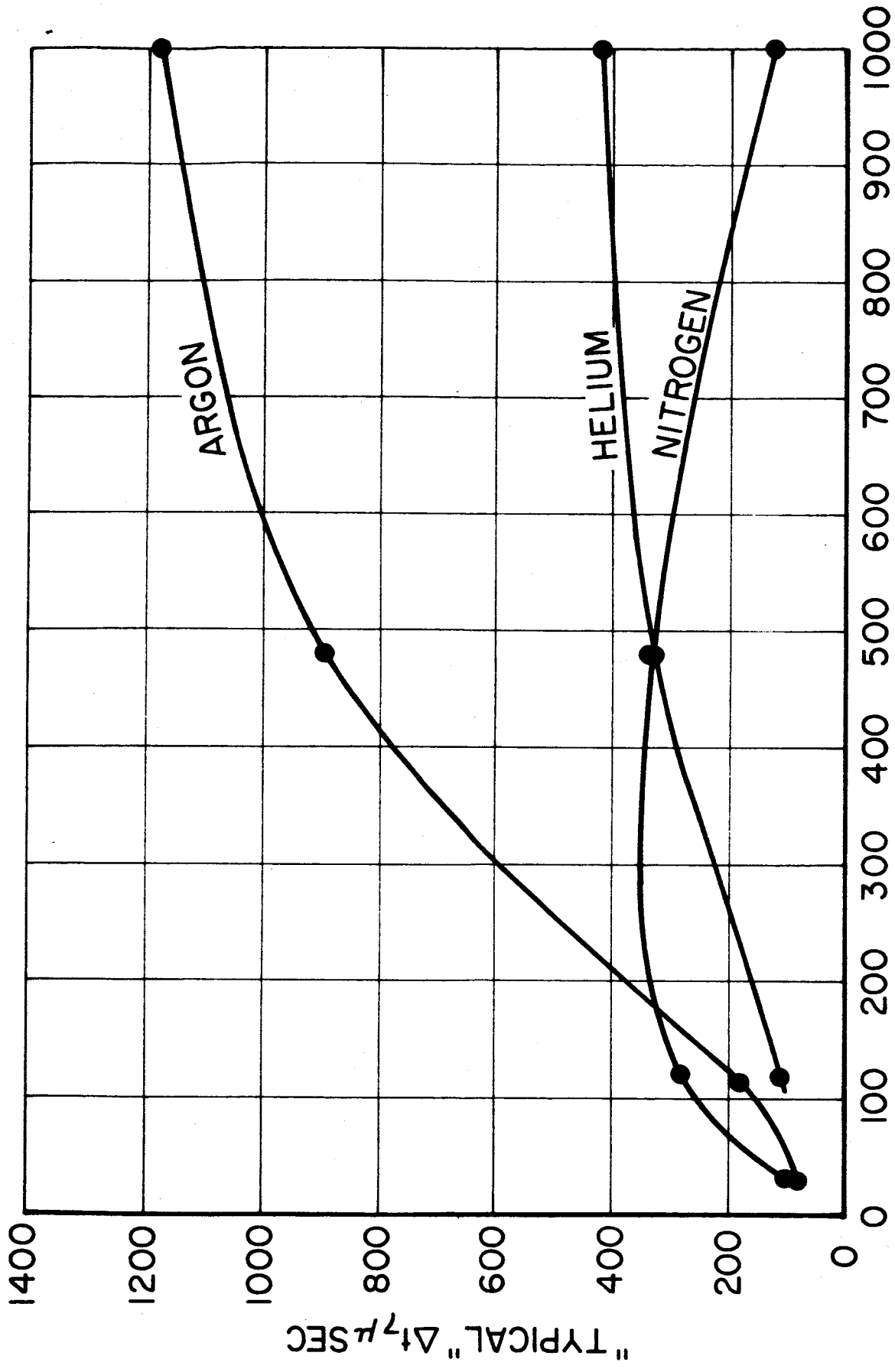

8" PINCH DISCHARGE, "TYPICAL" IONIZATION TIME vs PRESSURE, 70 GC

FIGURE 42

V. SPECTROSCOPY
(vonJaskowsky, Hermann)

In some earlier spectroscopic work, the presence of neutral, singly, and doubly ionized atomic lines in 8" pinch discharges in argon, nitrogen, and helium was established (4,5). Subsequently, the progression of various spectral lines through the luminous fronts was determined by photoelectric monitoring of the appropriate spectral region (13). During the present reporting period, the same photoelectric arrangement was used to monitor a representative portion of the emitted continuum radiation. In a series of discharges in 30 μ, 120 μ, 480 μ, and 1920 μ of Argon, the continuum radiation was recorded simultaneously with the total light profile at five radial stations from the periphery to the center of the discharge chamber. The total light pulse, which served as a local time calibration for the other signal, was obtained by reflecting a small fraction of the light out of the optical beam with a thin glass plate as shown in the sketch below. The remaining flux continued through a grating monochromator to another photomultiplier observing the selected spectral region emerging from the exit slit.

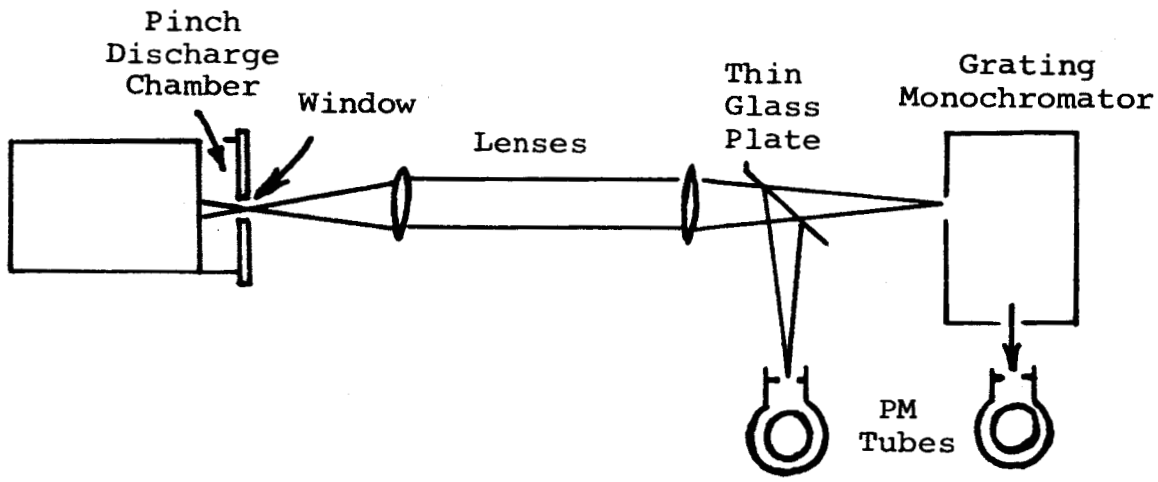

For this study the continuum in a 5 Å band around 4750 Å was found to be a suitable region well free of other lines whose absence was confirmed by recording the emitted intensity in overlapping wavelength bands near the central location. In fact, over the wavelength range from 3500 Å to 5300 Å, the continuum radiation was found to vary little in intensity, thus supporting the assumption of its origin as "Brems" radiation.

The profile of the emitted continuum radiation was observed to follow approximately the contour of the total luminosity seen on streak pictures and Kerr cell photographs. Figure 43 exhibits the measurements of the maximum continuum intensity achieved in the luminous fronts at different radial stations. At 30 μ and 120 μ the continuum profile did not reproduce well at the periphery of repeated discharges. The continuum intensity was observed to increase strongly during the final portion of travel of the contracting luminous front. The highest absolute intensity was attained in the discharge in 120 μ argon, indicative of a correspondingly high electron density in the pinch. The continnum intensities in discharges at the other pressures differed by less than a factor of two from the discharge in 120 μ. The measurements of continuum intensity of the pinched discharges in the center at different initial pressures of argon are shown in Fig. 44. The interpretation of these measurements in terms of electron densities is unfortunately not possible without some further information about the degree of ionization, the electron temperature, and an absolute calibration of the intensities.

In the earlier work (13), a separation of the peak of the AII intensity ahead of the AIII and the continuum peaks at the half-radius position was mentioned. In the present series of experiments, the total white light signal at the 3/4 R_o location was observed to peak ahead of the peak of the continuum radiation. This separation may correspond to the previously observed effect at the one-half radius position and may similarly be interpreted as evidence of the progress of ionization within the luminous front.

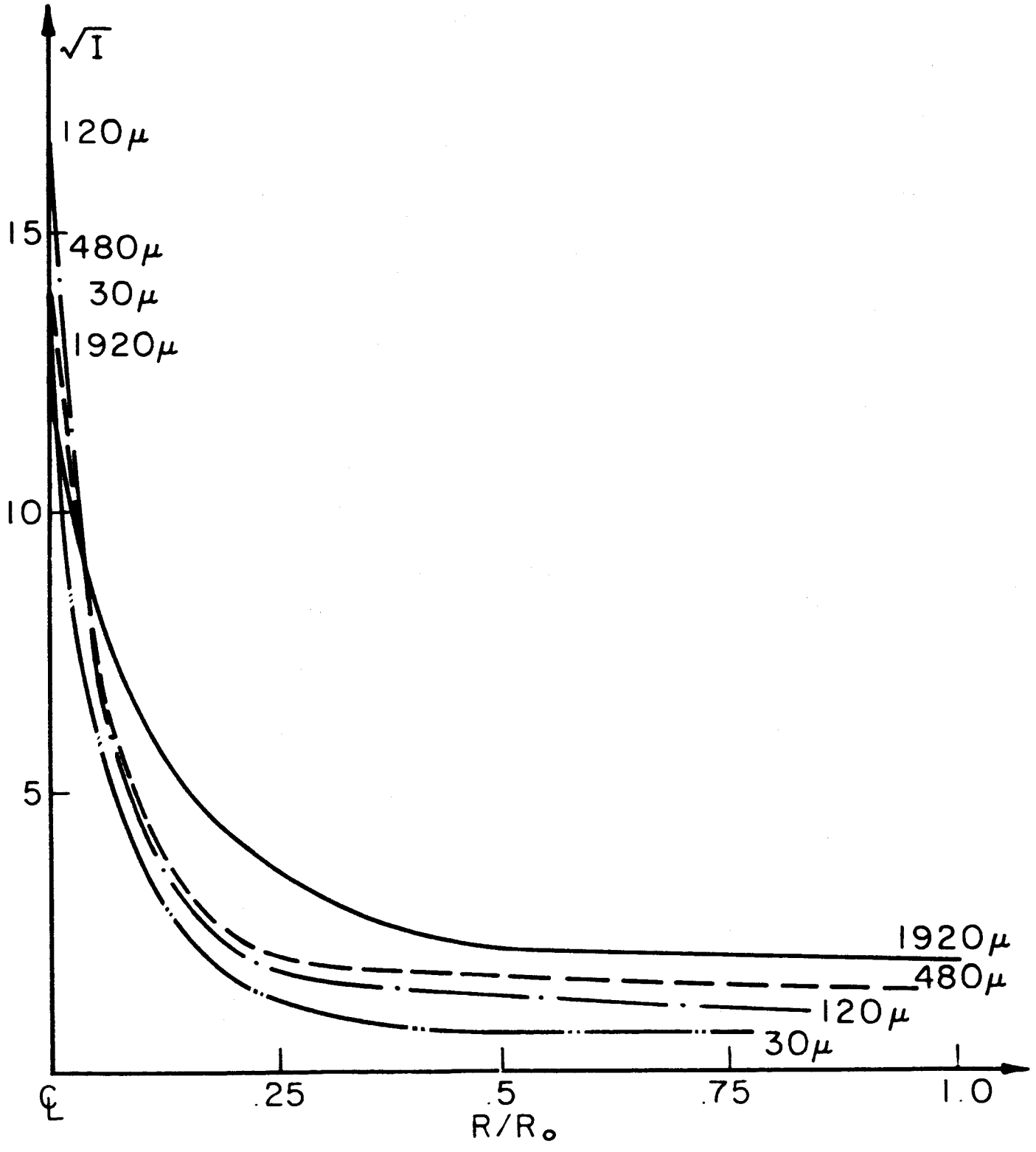

MAXIMUM CONTINUUM INTENSITY IN LUMINOUS FRONT AT 4750 Å

FIGURE 43

AP25-JPR-4022-65

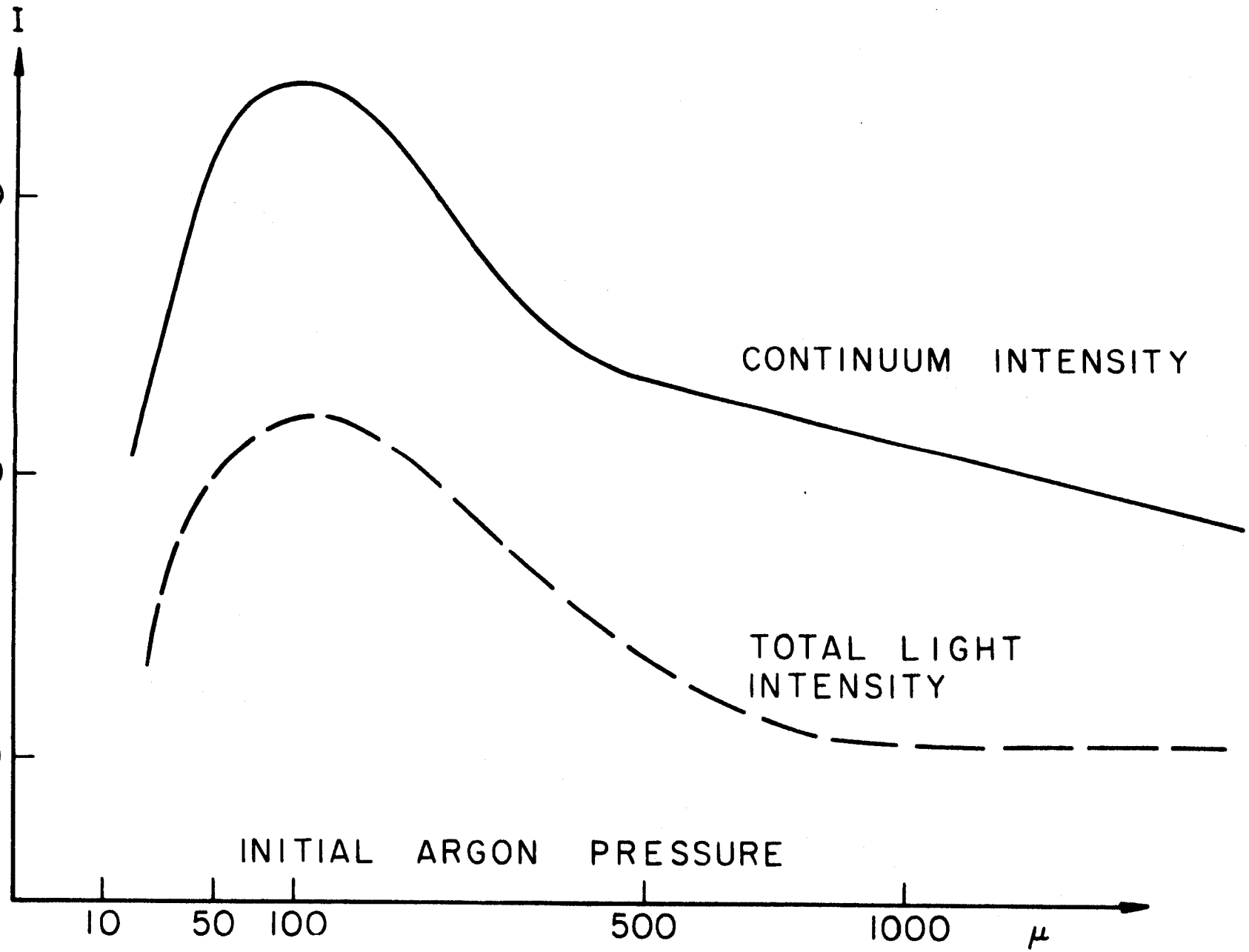

FIGURE 44 MAXIMUM CONTINUUM INTENSITY IN CENTER OF PINCH AT 4750 Å

VI. OTHER STUDIES, SUMMARY, AND PLANS

For the sake of brevity, we will not report in detail here on several other experimental and theoretical aspects of the program which are currently in progress. Some of these will be discussed in separate reports and papers to be issued in the coming months, some will form Ph.D. and Masters Theses, and some will be described in the next semi-annual report. These include: 1) Experimental studies of the breadth of applicability of snow-plow scaling relations (Eckbreth); 2) Experimental study of energy partition in the pinch discharge (Holzhauer, Turchi); 3) Magnetic probe determination of three-dimensional current density distributions in the pinch discharge (Burton); 4) Development of miniature Rogowsky coil probes (Wright); 5) Electric probe studies of interior charge densities (19)(Corr); 6) Development of theoretical cylindrical shock and gasdynamic models suitable for machine computation of the transient flow field in the pinch (Rowell); 7) Theoretical study of the dynamical efficiency of pulsed plasma accelerators (Black, Jahn); and 8) Assorted feasibility studies on new diagnostic and instrumentation techniques (Staff).

Each of these topics, as well as those discussed in more detail in the previous sections, will continue to be studied during the coming six months. The pattern of collaboration of these various efforts is now quite evident, and the steady increase in our understanding of the basic processes of pulsed plasma acceleration which is attained by the comparison and interaction of these separate studies is highly rewarding. For the first time since the start of this program, we find ourselves in substantial control of the basic phenomena under study, to the extent that we can now produce, at our discretion, a range of pulsed plasma interactions with obvious relevance to propulsion. Indeed, these interactions are found to be sufficiently intense and efficient to offer genuine optimism for ultimate implementation into useful space thrustors.

REFERENCES

1. "Proposed Studies of the Formation and Stability of an Electromagnetic Boundary in a Pinch." Proposal for NASA Research Grant NsG-306-63, 5 March 1962.

2. First Semi-Annual Progress Report for the period 1 July 1962 to 31 December 1962, Research Grant NsG-306-63, Aeronautical Engineering Report No. 634, Princeton University, Princeton, New Jersey.

3. "The Plasma Pinch as a Gas Accelerator," AIAA Electric Propulsion Conference, 11-13 March 1963, preprint 63013.

4. Second Semi-Annual Progress Report for the period 1 January 1963 to 30 June 1963, Research Grant NsG-306-63, Aeronautical Engineering Report No. 634a, Princeton University, Princeton, New Jersey.

5. "Structure of a Large-Radius Pinch Discharge," AIAA Journal 1, 8, 1809 (1963).

6. "Gas-Triggered Inverse Pinch Switch," Review of Scientific Instruments 34, 12, 1439 (1963).

7. "A Gas-Triggered Inverse Pinch Switch," Technical Note, Aeronautical Engineering Report No. 660, Princeton University, Princeton, New Jersey.

8. "Pulsed Electromagnetic Gas Acceleration," paper No. II, 8, Fourth NASA Intercenter Conference on Plasma Physics in Washington, D. C., 2-4 December 1963.

9. Third Semi-Annual Progress Report for the period 1 July 1963 to 31 December 1963, Research Grant NsG-306-63, Aeronautical Engineering Report No. 634b, Princeton University, Princeton, New Jersey.

10. "Pulsed Electromagnetic Gas Acceleration," a renewal proposal for extension of NASA Research Grant NsG-306-63, Princeton University, Princeton, New Jersey, 15 January 1964.

11. "Current Distributions in Large-Radius Pinch Discharges," AIAA Bulletin 1, 1, 12 (1964).

12. "Current Distributions in Large-Radius Pinch Discharges," AIAA Aerospace Sciences Meeting, New York, New York, 20-22 January 1964, preprint 64-25.

13. Fourth Semi-Annual Progress Report for the period 1 July 1964 to 31 December 1964, Research Grant NsG-306-63, Department of Aerospace and Mechanical Sciences Report No. 634c, Princeton University, Princeton, New Jersey.

14. "Current Distributions in Large-Radius Pinch Discharges," AIAA Journal 2, 10, 1749 (1964).

15. "Gas-Triggered Pinch Discharge Switch," The Review of Scientific Instruments 36, 1, 101 (1965).

16. "Gas-Triggered Pinch Discharge Switch," Princeton Technical Note No. 101, Department of Aerospace and Mechanical Sciences, Princeton University, Princeton, New Jersey, July 1964.

17. "Exhaust of a Pinched Plasma from an Axial Orifice," AIAA Bulletin 1, 10, 570 (1964).

18. "Exhaust of a Pinched Plasma from an Axial Orifice," AIAA Second Aerospace Sciences Meeting, New York, New York, 25-27 January 1965, paper no. 65-92.

19. "Double Probe Studies in an 8" Pinch Discharge," M.S.E. Thesis of J. M. Corr, Department of Aerospace and Mechanical Sciences, Princeton University, September 1964.